Lessons Learned on the Use of Data Surfaces for Ffowcs Williams-Hawkings Calculations: Airframe Noise Applications

André F. P. Ribeiro[1]
Dassault Systèmes *GmbH, 70563, Stuttgart, Germany*

Mehdi R. Khorrami[2]
NASA Langley Research Center, Hampton, VA, 23681, USA

Ryan Ferris[3]
Dassault Systèmes, *Long Beach, CA, 90802, USA*

Benedikt König[4]
Dassault Systèmes *GmbH, 70563, Stuttgart, Germany*

Patricio A. Ravetta[5]
AVEC Inc., Blacksburg, VA 24060, USA

The use of integral solutions to the acoustic-analogy-based Ffowcs Williams-Hawkings (FW-H) formulation is the de facto industrial and academic approach for assessing far-field acoustic behavior from airframe noise simulations. The methodology utilizes time-accurate flow variables obtained at arbitrary data surfaces to determine far-field spectra. The solid surface approach, where the time history of pressure is recorded on the surface of the aircraft, is generally preferred. Permeable surfaces, where pressure and velocity are recorded on a user-defined surface enclosing the aircraft, are also used. This paper seeks to share some of the valuable lessons we learned over the past several years on the limitations of the FW-H formulation and best practices for its successful application. We show results for various configurations comprising isolated landing gears, a business jet, a large commercial transport, and a generic low boom supersonic prototype, all at landing conditions. We demonstrate that the solid FW-H approach has significant accuracy limitations for most realistic cases and that the permeable FW-H approach may also fail in specific scenarios, requiring additional costly steps to extract the correct far-field noise spectra. Suggested guidelines for proper FW-H calculations are also given.

I. Nomenclature

CFD	=	Computational Fluid Dynamics
FW-H	=	Ffowcs-Williams and Hawkings
GLBC	=	Generic Low Boom Concept
LBM	=	Lattice-Boltzmann Method
LCT	=	Large Civil Transport

[1] Industry Process Senior Specialist, SIMULIA Aerospace & Defense, AIAA Member.
[2] Senior Scientist, Computational AeroSciences Branch, Associate Fellow AIAA.
[3] SIMULIA Industry Process Consultant, SIMULIA NAM 3DX Fluids, AIAA Member.
[4] Fluids Industry Process Expert Specialist, AIAA Member.
[5] Co-owner, Chief Research Engineer, Senior Member AIAA.

LG = Landing Gear
MLG = Main Landing Gear
NLG = Nose Landing Gear
VLES = Very Large Eddy Simulation

II. Introduction

Application of scale-resolving computational methodologies to the study of airframe noise has become an important tool for the prediction and mitigation of the impact of civil transport operations on community noise. These high-fidelity simulations have progressed rapidly from simple, model-scale airframe components to real-world, complete aircraft with extreme geometric complexities [1]. Due to prohibitive computational costs, finer spatial and temporal resolution of the flow field are invariably restricted to a relatively small volume surrounding the airframe component(s) of interest. Therefore, for prediction of far-field noise signatures, near-field flow solutions are used in conjunction with propagation formulations to calculate the signal at distant locations on the ground. The Ffowcs Williams-Hawkings (FW-H) equation [2] and the integral representation of its solution developed by Farassat [3] have become the preferred propagation method for use with airframe noise simulations.

Input to the FW-H formulation can be fluctuating pressures on the airframe (solid) surface or unsteady flow parameters on an arbitrary, penetrable surface enclosing a limited volume adjacent to the airframe [4]. Both solid and permeable data surfaces have advantages and disadvantages that pose numerous challenges to the process of accurately predicting far-field noise characteristics. A brief account of the key consequences of using both surface types is presented here. A full-volume formulation is also available, but it is typically too expensive for practical use [5], hence we will not consider it here.

Relative to using a permeable acoustic data surface, the solid surface formulation provides a path that is more affordable computationally. For most configurations, the highest spatial and temporal resolutions occur adjacent to the model solid surfaces. Thus, the simulated data can be sampled at higher rates to produce noise predictions that cover a broader frequency range. In addition, the solid surface represents a "clean" formulation that can be easily implemented since the position and orientation of the aircraft surfaces are well defined, closed, fixed, and known a priori. Also, this formulation is not strongly influenced by wake resolution [6] and pressure is the only variable to be recorded and processed. The main disadvantage of using solid surface data is that quadrupole effects are neglected. Quadrupole effects include volumetric acoustic sources and any propagation phenomena beyond those described by the convective wave equation for a uniform medium. Examples are presented demonstrating that the formulation becomes problematic when shielding is present or when complex geometries (e.g., aircraft undercarriage system) are involved. In these instances, the prevalent flow nonlinearities and nonuniformities contribute to inaccurate predictions when solid surface data are used.

The permeable data surface formulation is significantly more expensive computationally and its implementation vastly more complex since the extent, orientation, and position of the data surface are not known a priori. Thus, an iterative process is required to arrive at a surface with the desired attributes [5]. Ultimately, to attain the best predicted far-field noise results, the permeable surface must be tailored to accommodate the aircraft type and conditions of interest. One of the more concerning difficulties with this formulation relates to hydrodynamic flow structures (wake fluctuations) exiting the permeable surface, as these may be manifested as numerically generated noise sources [7]. Much research is being conducted to understand and reduce this type of numerical noise [8] [9] [10] [11] [12] [13] [14]. The most important advantage of this formulation is that quadrupole and shielding effects should be addressed correctly when an appropriate permeable surface is used. The accuracy of the predicted far-field noise depends on the nature and extent of the volume enclosed by the permeable surface. So, if said surface is placed too close to the aircraft, while computationally attractive, the predictions will suffer from some of the disadvantages associated with solid surfaces. Furthermore, a permeable surface that encloses an expansive volume surrounding the aircraft will require costly maintenance of fine spatial and temporal resolutions within a large volume, thus increasing solution turn-around time and computational cost. Applications such as jet noise, where the sources are mostly quadrupoles, must use permeable data surfaces and some best practices have been identified for such cases [15].

Most early airframe noise studies used simple airframe geometries and relied exclusively on solid surface data to make the simulations affordable. However, when more complex airframe components and configurations are considered, the use of solid data surfaces yields inaccurate far-field noise spectra. In Ref. [16], some inaccuracies of the solid surface formulation, in particular for bodies where shielding effects are important, were demonstrated via examination of several relatively simple configurations.

Over the past 7-8 years, the present authors have conducted numerous airframe noise simulations for a wide array of configurations studied under various NASA projects. In this paper, we present results from a subset of those

configurations to illustrate some of the challenges encountered when different types of FW-H data surfaces are used and share some of the remedies we devised to improve the accuracy of far-field noise predictions.

III. Configurations and Test Cases

The selected configurations comprise a) model- and full-scale realistic landing gear in isolation, b) a full-scale, complete business jet, c) a full-scale, complete Boeing 777-300ER aircraft, and d) a model-scale generic low boom concept (GLBC). All simulations were conducted for landing conditions. As one of the few groups that have adopted a FW-H permeable surface formulation for the prediction of noise from complex aircraft configurations, we have been fortunate to have access to measured acoustic data from wind tunnel and flight tests to validate the predicted results. A brief overview of the test cases is given in this section. Further details can be found in the references to the publications on each configuration.

A. Isolated Main Landing Gear (MLG) and Nose Landing Gear (NLG)

Isolated model- and full-scale landing gear for a large civil transport aircraft were investigated as precursors to full-scale investigations of a complete Boeing 777 aircraft. Initial studies on a high-fidelity, 26%-scale wind tunnel model of a B777 main landing gear were presented in Ref. [17], see Fig. 1(a). This model had also been extensively tested at the Virginia Tech Stability Wind Tunnel. The comparatively simple configuration was used to test and validate the simulation and post-processing approach – good agreement was achieved between measured and predicted far-field spectra over a wide frequency range. The model was also tested with a toboggan fairing that completely covered the gear axles and the wheel brake system [17].

Further refinement of the methodology was performed on the installed – but quasi-isolated – nose-landing gear with fully detailed, as-flown geometry [18], shown in Fig. 1(b). The forward location of the NLG, together with a clean-wing aircraft configuration, allowed very detailed comparisons between simulations and measured noise data from flight tests.

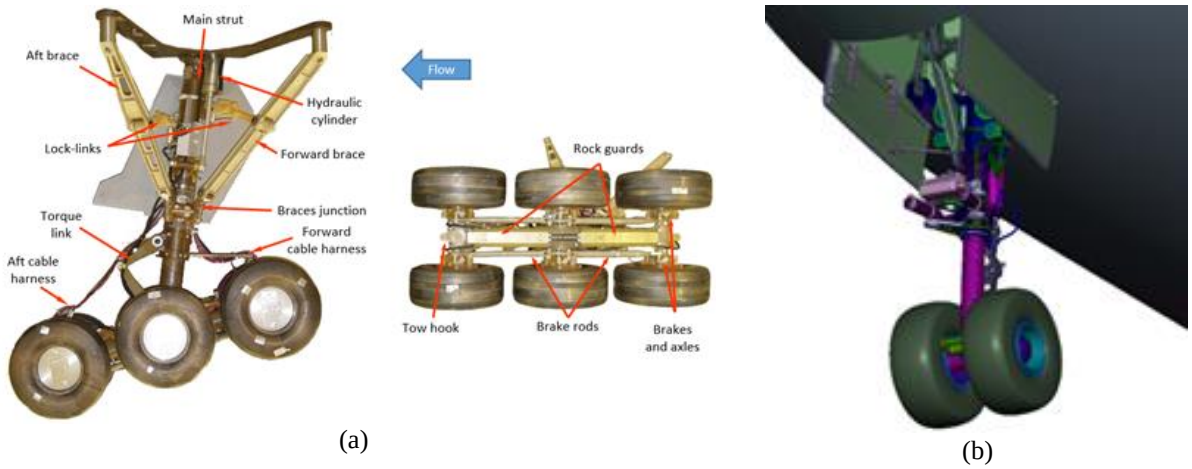

(a) (b)

Fig. 1 Isolated landing gear (a) 26%-scale wind tunnel model from Ref. [17], and (b) close-up of simulated full-scale NLG and gear bay from Ref. [18].

B. Gulfstream G-III Business Jet

The set of G-III test cases resulted from a comparative analysis between high-fidelity, full-scale, simulations and data acquired during the NASA Acoustic Research Measurements flight tests. The goals of these comparisons were to quantify the effectiveness of installed noise reduction concepts and to evaluate the capability of the simulation methodology to design and develop viable noise mitigation technologies. The aircraft model, shown in Fig. 2, is a laser-scanned Gulfstream G-III in two separate configurations. Computational and flight test data were analyzed with the base G-III aircraft: 1) fitted with the traditional Fowler flap system and, 2) fitted with an Advanced Compliant Trailing Edge (ACTE) flap system. A porous main landing gear (MLG) fairing, not pictured, was also used to study its effectiveness in reducing airframe noise during approach. The ACTE flap employed a continuous mold line surface that removed flap-side edges, flap gaps, flap tracks, and the associated mechanical components traditionally exposed to the free stream in a Fowler flap configuration.

Using the noise generated from the Fowler flap equipped G-III as a baseline, computational assessments were made on combinations of installed noise reduction concepts in Ref. [19]. Details on the simulation and flight test

results for both G-III configurations can be found in Ref. [20]. The effect of the porous MLG fairing on the noise generated by the Fowler flap equipped G-III aircraft was discussed in Ref. [21]. Finally, a summary of all flight and simulation results for this study was presented in Ref. [22].

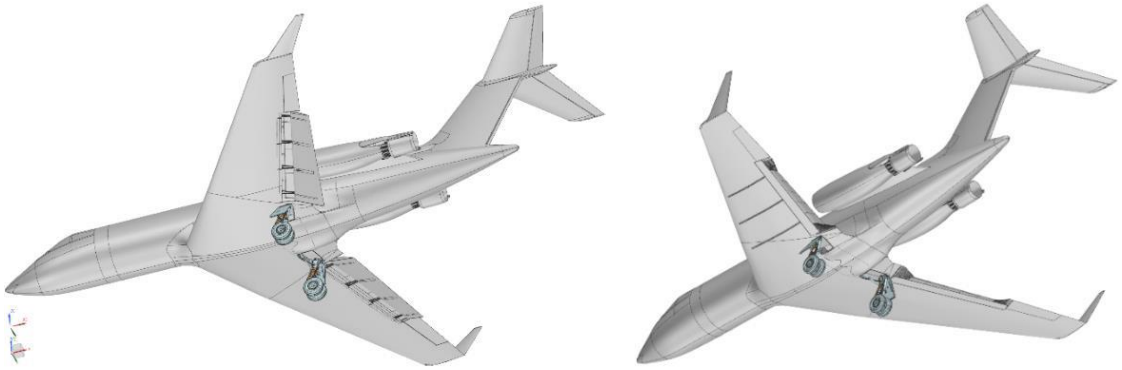

(a) (b)

Fig. 2 G-III with flaps and landing gear deployed: (a) Fowler flap system and (b) ACTE system [22].

C. Large Civil Transport (LCT)

A highly accurate representation of a full-scale, large civil transport (LCT), namely the Boeing 777-300ER, with as-flown nose and main landing gear was investigated in both a clean-wing and a landing configuration with high-lift devices deployed, as shown in Fig. 3. Extreme care was exercised to ensure that the NLG and MLG models faithfully replicated the full-scale landing gear as flown on the real aircraft. Simulated phased microphone array data were compared to Quiet Technology Demonstrator II (QTD2) flight test measurements. Overall good agreement of computed noise levels to the aircraft flyover measurements, well within the expected uncertainty band of the flight test, was found for emission angles that were not contaminated by residual engine noise.

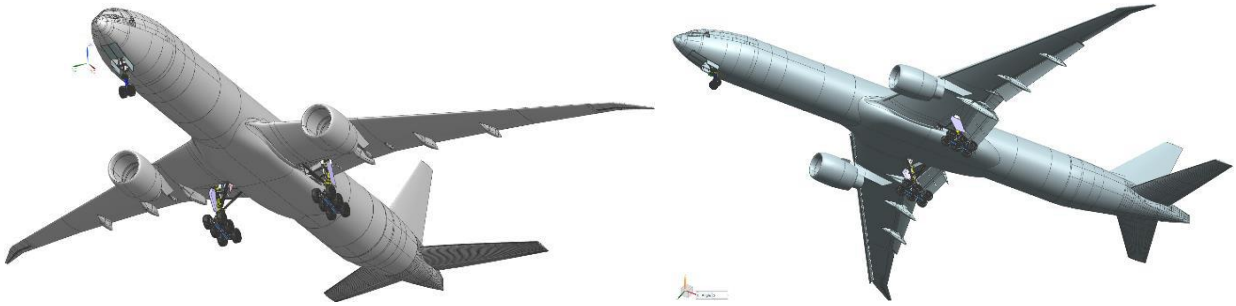

(a) (b)

Fig. 3 Full-scale B777-300ER aircraft with NLG and MLG deployed: (a) with high-lift devices retracted (clean wing) and (b) in landing configuration with high-lift devices deflected [23].

The LCT study was a very successful attempt at simulating the aeroacoustic behavior of a twin-aisle aircraft with an exceptionally high degree of geometric complexity and represented the first step toward fulfilling a grand challenge for airframe noise prediction. Details of the simulation setup are provided in Ref. [23], and validation against flight test data is given in Ref. [24]. Valuable insights gained from this study with regard to the application of FW-H data surfaces are documented in Ref. [25].

D. Generic Low Boom Concept (GLBC)

The GLBC, shown in Fig. 4, is a supersonic aircraft model designed by NASA. A 15%-scale model of the GLBC was tested in the Langley Research Center 14- by 22-Foot Subsonic Tunnel to determine its low-speed aerodynamics in preparation for the flight tests of the X-59 supersonic demonstrator. The GLBC is part of NASA's efforts to develop methods and tools to support the new era of commercial supersonic flight. Although no experimental acoustic data are available for this model, aerodynamic data were obtained for configurations with flaps deployed and retracted, and landing gear deployed and stowed. The measurements were used for validation of the aerodynamic simulations [26]. Aeroacoustic simulations of the GLBC aircraft in several configurations are described in Ref. [27]. Synthetic phased

microphone array data generated from these simulations were used to perform beamforming studies [28], which allowed the major airframe sources to be identified for more accurate definitions of the far-field noise spectra.

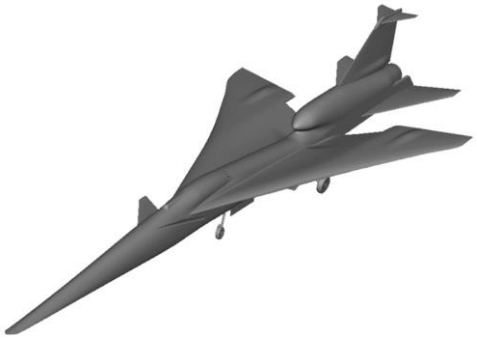

Fig. 4 GLBC with flaps and landing gear deployed (from Ref. [27]).

Details on the GLBC computational setup are provided in Ref. [26], where aerodynamic simulations in the wind tunnel and free air are introduced, analyzed, and validated. Information on the free-air aeroacoustic simulations and computed far-field noise spectra from single-microphone results are given in Ref. [27]. A description of the experiments, comparison of aerodynamic simulations to experimental data, and analysis of the synthetic phased microphone array data are provided in Ref. [28].

IV. Methodology

The main simulation components presented in this work are the CFD solver, the FW-H tool, and the beamforming software. They are described in this section.

A. Flow Solver

The Lattice-Boltzmann method (LBM) [29] solver SIMULIA PowerFLOW® was used for all simulations presented herein. The LBM is an attractive alternative to Navier-Stokes solvers [30] due to the simple mathematics involved, which do not require gradient calculations and are mostly done in a cell-local manner, leading to performance that is 1-3 orders of magnitude faster than traditional solvers [7] and has good scalability on parallel computers. The LBM is typically solved on Cartesian grids [31], which allow for very robust mesh generation on extremely complex geometries. The relatively large wall spacing requires wall models to describe boundary layers, but PowerFLOW uses well-validated, extended wall models with pressure gradient effects [32]. Some of the unique features of PowerFLOW are surface elements, or surfels, which are a more accurate alternative to standard immersed boundary layer methods [33]; and the very large eddy simulation (VLES) approach to turbulence modelling [34], which reduces a k-ε RNG [35] model's eddy viscosity based on how resolved the flow structures are. Extensions for compressibility effects are used [36], as the flow fields in the majority of simulations reported in this paper reach relatively high local subsonic Mach numbers.

B. Acoustic Propagation

SIMULIA PowerACOUSTICS® [37] was used in this work to propagate the noise from the near field to the far field. The software is based on a forward-time solution [38] of Farassat's formulation 1A [3]. Solid and permeable integration surfaces are supported, along with the inclusion of convective effects [39]. The code was validated with third-party (PSU-WOPWOP) and in-house NASA FW-H reference software applied to a generic configuration [40].

C. Noise Source Identification

Computed pressure records obtained from PowerACOUSTICS were processed using AVEC's Phased Array software [41]. Beamforming in the frequency domain was used to process all synthetic array data. Flow convection effects were included in the FW-H propagation and beamforming process. Diagonal removal and array shading were used to improve the results [42]. Beamforming output was post-processed with the CLEAN technique [43]. Integration results were computed from CLEAN maps obtained with "zero-resolution," thus avoiding the need for normalization. For visualization purposes, however, the CLEAN acoustic maps presented here were generated using an artificial resolution based on model size.

V. Limitations of Solid Data Surfaces

As mentioned in section II, the solid data surface formulation is not an appropriate choice when shielding effects are important. Theoretically, for low Mach numbers, if a surface produces noise and another surface is between that noise source and the microphones, the pressure fluctuations on the two surfaces will interfere destructively when the solid FW-H approach is used, capturing accurately the shielding effects. However, even modest amplitude or phase differences between the actual pressure fluctuations incident on these surfaces and their expected theoretical values can yield incorrect estimates of the shielding effects.

If the noise generated by a source is diffused or dispersed by the CFD solver before it reaches the shielding surface, the cancelling effect will be affected. However, these errors would be manifested mostly near or at frequencies beyond which there is insufficient spatial-temporal resolution. Volumetric (quadrupole) sources, albeit weak for the Mach numbers studied here, can also affect the perfect cancelling of sources and shielding surfaces.

Another mechanism that can affect solid surface results is convection. With the Farassat formulation 1A, a uniform flow with freestream velocity is assumed, which is incorrect in regions of flow acceleration/deceleration or separation. All problems of airframe noise include convection and the vast majority involve separated flows. Again, even small differences in amplitude and phase due to the solid data surfaces not being in quiescent/uniform flow regions can adversely affect interference and shielding effects.

In this section, we show several examples where solid data surfaces generate incorrect noise signatures and discuss some of the underlying assumptions and mechanisms.

A. Isolated MLG and NLG

To assess the differences in noise caused by data surface type, the spatial resolution maintained within the permeable data surface was extended to enclose a series of sampling locations, or CFD probes, along the overhead direction. Fig. 5 compares the baseline MLG noise produced by the data surfaces in the overhead position (90°) with noise extracted directly from the simulation at the same point, that is, the probe located nearest the MLG and shown in the image on the right side of the figure. Observe that the permeable surface spectrum matched that from the direct probe very well, while results from the solid surface tended to overpredict noise. Besides the obviously increased high-frequency broadband levels, there is also a peak in the solid surface results at 1000 Hz, which beamforming maps showed to originate from the region around the middle axle.

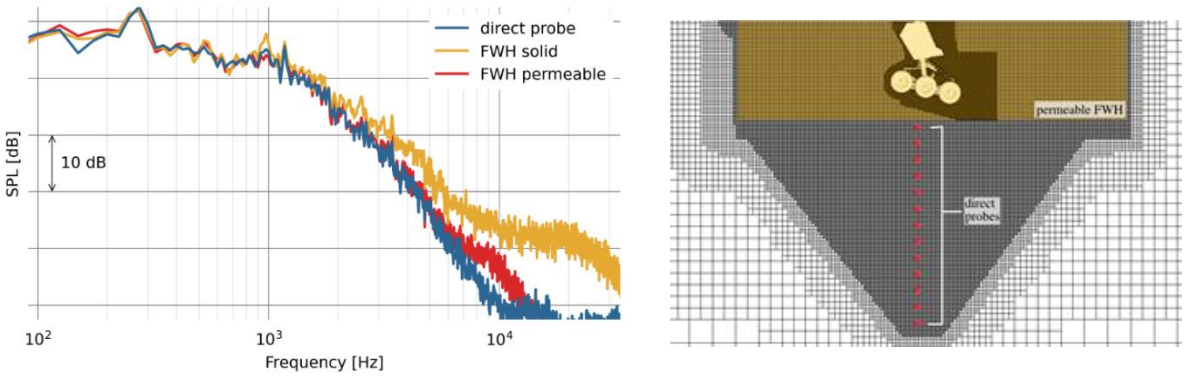

Fig. 5 Isolated baseline MLG noise spectra at overhead from data surfaces and direct probe (from Ref. [17]).

For the isolated MLG, the main mechanism for noise reduction was aerodynamic shielding, since the toboggan covered the brake cylinders, brake rods and other components in the truck. Beamforming of phased array data produced by the simulations allows a visual comparison of the differences among the noise sources. As seen in Fig. 6, maps from synthetic array pressure records sampled at the sideline and overhead directions indicate that with a solid acoustic data surface the noise emanating from the main strut effectively radiates through the side door, and that noise from the components in the truck radiates through the toboggan. For the reasons discussed in the introduction to this section, acoustic shielding effects are missed by the solid data surface approach.

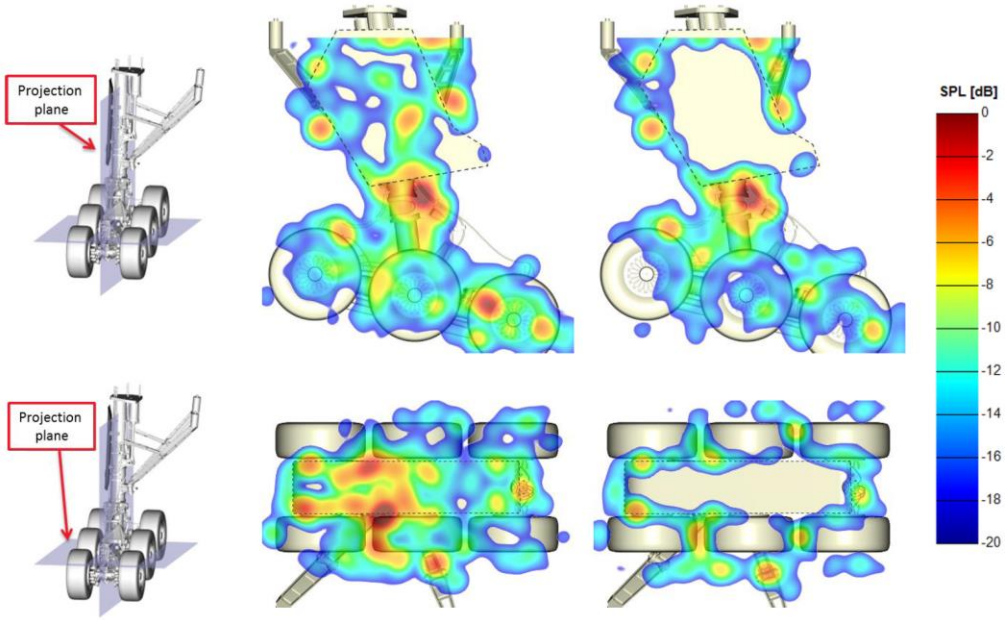

Fig. 6 LCT MLG with toboggan fairing. Conventional beamforming maps at 3 kHz. Left maps used solid surfaces, right maps used permeable surfaces (from Ref. [17]).

As a prelude to the full-aircraft simulations, the isolated NLG was an ideal testbed to conduct an extensive examination of the prominent trends and issues that may affect the accuracy of the predicted far-field noise signature. The orientation and extent of the permeable data surface used for the NLG simulations are depicted in Fig. 7. As seen in this figure, the surface designed to encompass all significant flow fluctuations generated by the NLG contained seven end caps to diminish, through averaging, the effect of hydrodynamic perturbations exiting the volume. The predicted spectra from the solid[6] and permeable data surfaces at a near-field location in the overhead position are shown in Fig. 8. Also included in this figure is the spectrum extracted directly from the CFD data (direct probe) at the same location (blue circle in the image on the right). As done for the MLG, the spatial resolution maintained within the permeable data surface was extended to enclose a series of CFD probes along the overhead and sideline directions. From Fig. 8, observe that the spectrum based on solid surface data produced significantly higher noise levels across the entire frequency range. The spectrum obtained from the direct CFD probe closely matched the permeable data surface spectrum at low and moderate frequencies, corroborating the appropriateness of permeable data surface results. Above 1600 Hz, the direct probe spectrum shows lower noise levels relative to the permeable data surface due to numerical diffusion (resolution) of the propagating waves.

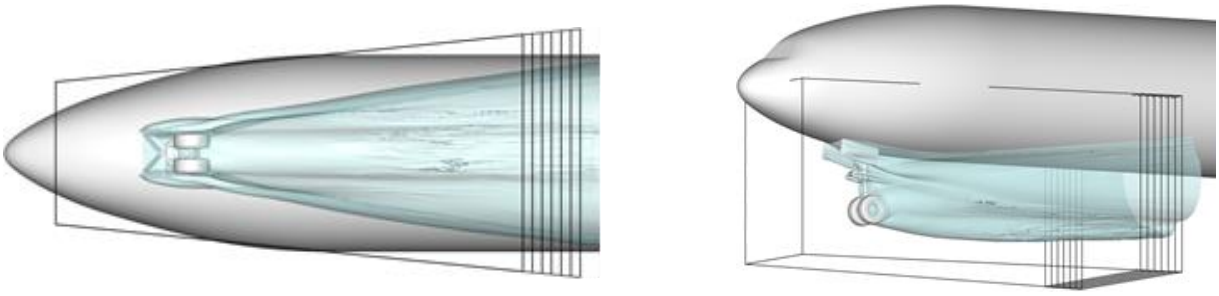

a) bottom view b) side view

Fig. 7 Permeable data surface for NLG. Light blue region corresponds to the isosurface of 1% standard deviation of velocity magnitude fluctuations (from Ref. [18]).

[6] The solid surface used during the simulations comprised the entire aircraft surface (cruise wing, fuselage, and empennage). However, since the mesh resolution downstream of the permeable surface was substantially coarser, very little unsteady pressure was observed on the rest of the aircraft surface.

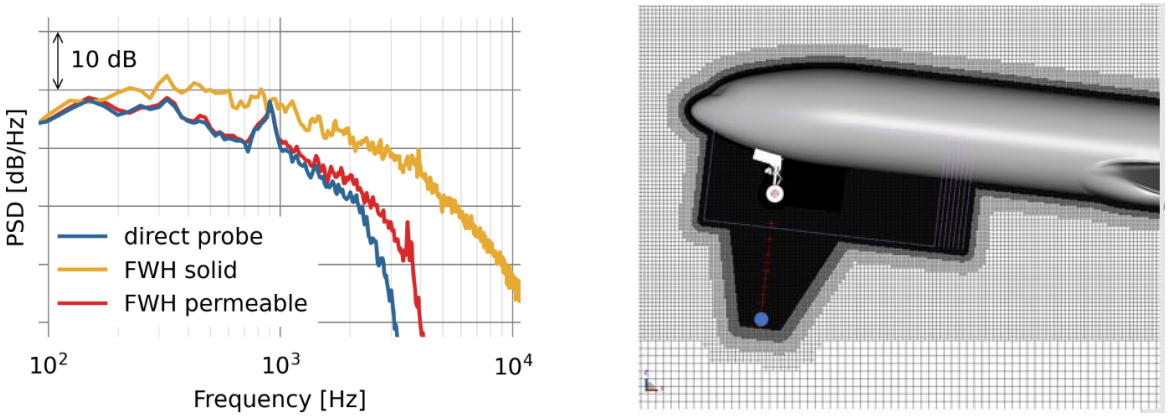

Fig. 8 NLG spectra from data surfaces and direct CFD probe at a near-field location. Computational mesh at symmetry plane and position of near-field probe (solid blue circle) are shown in the right image (from Ref. [18]).

We examined several potential causes for the higher noise levels observed in the solid surface spectrum. Landing gear cavities are known to produce elevated noise levels (both tonal and broadband) when the fluctuating pressures on the cavity walls are used. To determine the impact of the NLG cavity on the near-field noise spectrum, we repeated the simulation with the gear deployed and the cavity opening closed. The overhead spectra obtained from the closed-cavity configuration are compared with the open-cavity results in Fig. 9. As anticipated, closing the cavity opening substantially reduced the solid surface noise levels at frequencies below 1000 Hz. Above this frequency, the spectrum remains relatively unaffected. Conversely, except at very low frequencies, closing the gear cavity did not affect the spectra from the permeable data surface nor the direct probe. Although not shown, similar trends were noted in the sideline direction. These observations reinforce the facts that a) the cavity noise signature is not captured properly by the solid surface data and b) cavity noise alone does not account for overprediction of the solid surface noise levels. To further explore the underlying cause of solid surface overprediction, nearfield synthetic microphone arrays comprised of eight hundred elements each were placed in the overhead, sideline, and forward directions, as described in Ref. [25]. Reproduced from Ref. [25] are sample CLEAN maps obtained from solid and permeable surface pressure records (Fig. 10). The sideline maps clearly illustrate the inability of the solid surface formulation to account correctly for shielding effects: because of the NLG door and wheel, the noise sources in the cavity and on the gear axle should be hidden and invisible to an observer in the sideline direction. The complex geometry of the NLG and the presence of numerous subcomponents of various sizes and shapes significantly shield the sources in the overhead and other directions as well. Sample CLEAN maps from the near-field array in the overhead direction are provided in Fig. 11. Both frontal and rear views of the 3D maps show significant differences in the source distribution, with the solid surface maps depicting additional sources in the cavity and along the main post of the NLG. Note here that correct interpretation of the source distributions in three-dimensional (3D) beamform maps of the NLG requires careful consideration, as shielding and other non-linear effects may not be obvious.

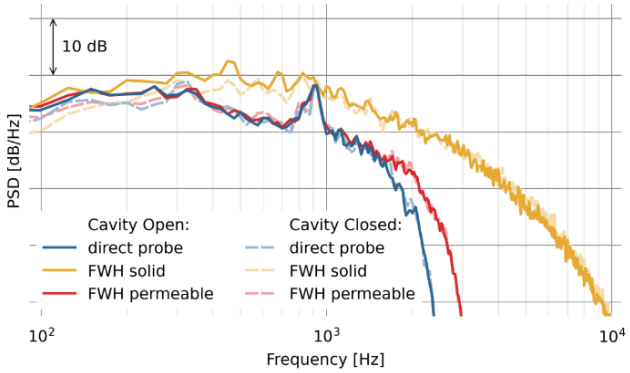

Fig. 9 Effect of cavity closing on NLG spectra obtained from solid and permeable surfaces and direct CFD probe.

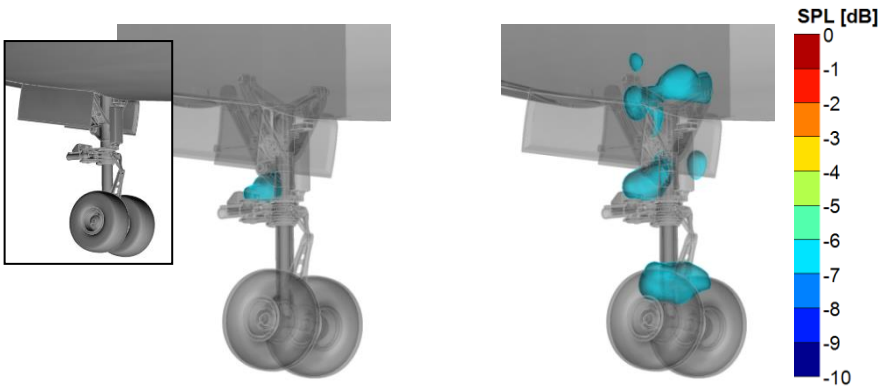

a) Permeable surface b) Solid surface

Fig. 10 NLG CLEAN 1/12th octave band isosurfaces from sideline array (7 dB from peak level) at 4.25 kHz (from Ref. [25]).

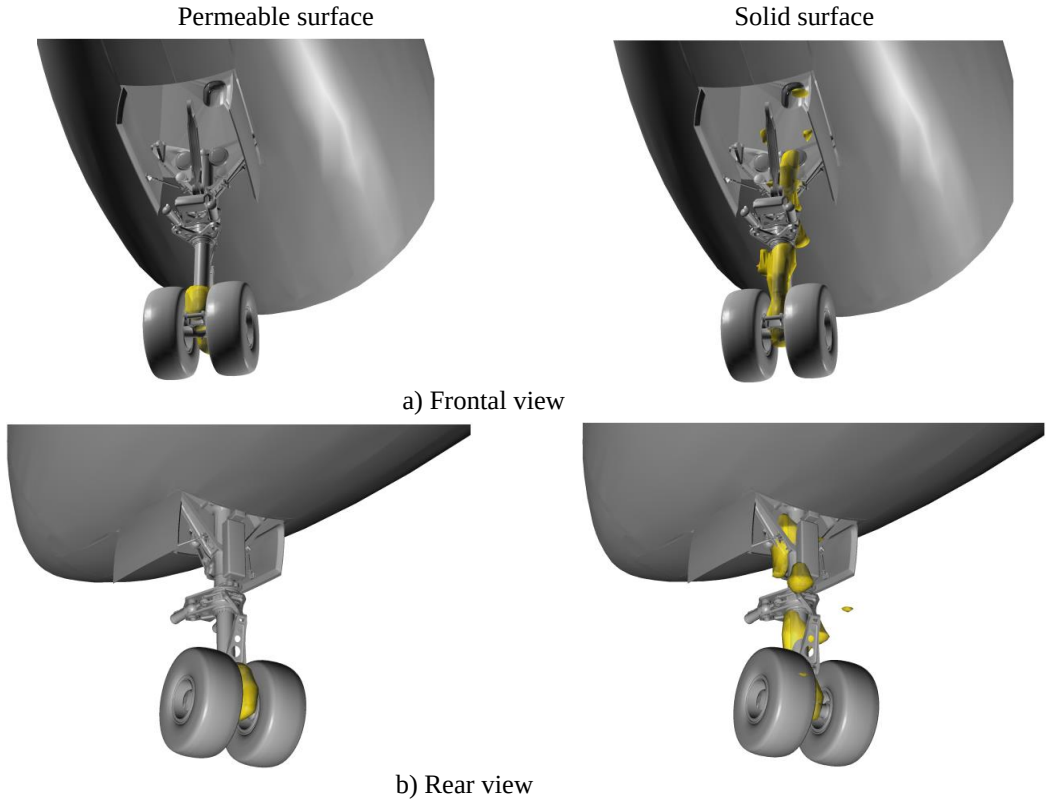

a) Frontal view

b) Rear view

Fig. 11 NLG CLEAN 1/12th octave band isosurfaces from overhead array (6 dB from peak level) at 2.8 kHz. Left column permeable surface and right column solid surface maps.

B. G-III

The primary set of G-III simulations involved configurations that did not include the nose landing gear (see Fig. 2), since the intended noise reduction concepts were applied to, and evaluated on, the G-III main landing gear. Given the forward position and relatively isolated nature of the NLG, its omission did not affect the noise signature of other airframe components and allowed the simulations to be performed at a reduced cost or higher spatial resolution.

A nominal permeable surface viable for the two G-III configurations of interest (Fig. 2), obtained after several iterations, is shown in Fig. 12. This surface was deemed to incur reasonable computational costs (spatial resolution) while containing the entire aircraft. Sample CLEAN beamform maps from the solid and permeable data surfaces for the G-III equipped with ACTE flaps (Fig. 2b) are shown in Fig. 13. A ground array comprised of 185 microphones used during the flight test campaigns was employed to process and analyze the synthetic pressure records. As can be

seen in Fig. 13, at low to moderate frequencies, both solid and permeable data surface maps produced very similar source distributions and strengths. However, at higher frequencies, while maintaining similar distributions, the sources based on the permeable data surface show lower noise levels compared to those obtained from the solid surface. This is to be expected, as acoustic waves with shorter wavelengths will experience higher diffusion (spatial resolution) effects as they propagate through the volume before reaching the permeable surface. To determine the noise footprint of the G-III aircraft, several regions were devised for tailored integration of the source maps (see Fig. 14). For the G-III equipped with ACTE flaps (i.e., with flap noise sources eliminated), the "MLG" integration region was used to extract the main gear contribution to the far-field noise signature. For the G-III with Fowler flaps, the "WingsNg" integration region was used to extract the combined main gear and flap contribution to the far-field noise. The square region enclosed by the black line outlines the entire beamform plane "Whole Grid" that was used to obtain the total noise for the aircraft.

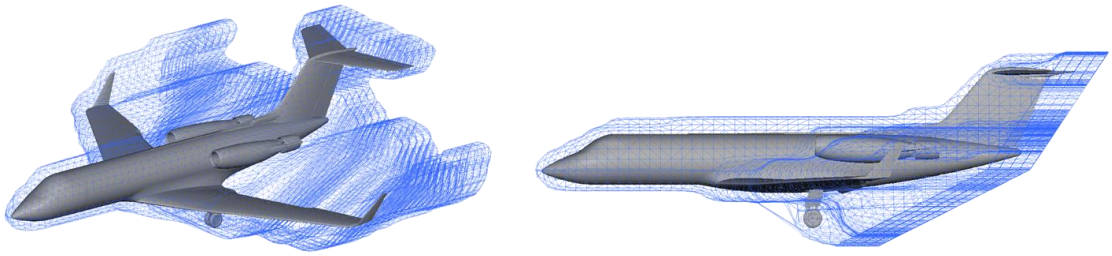

Fig. 12 Permeable surface used for fine-resolution simulation as shown on the ACTE configured G-III (from Ref. [19]).

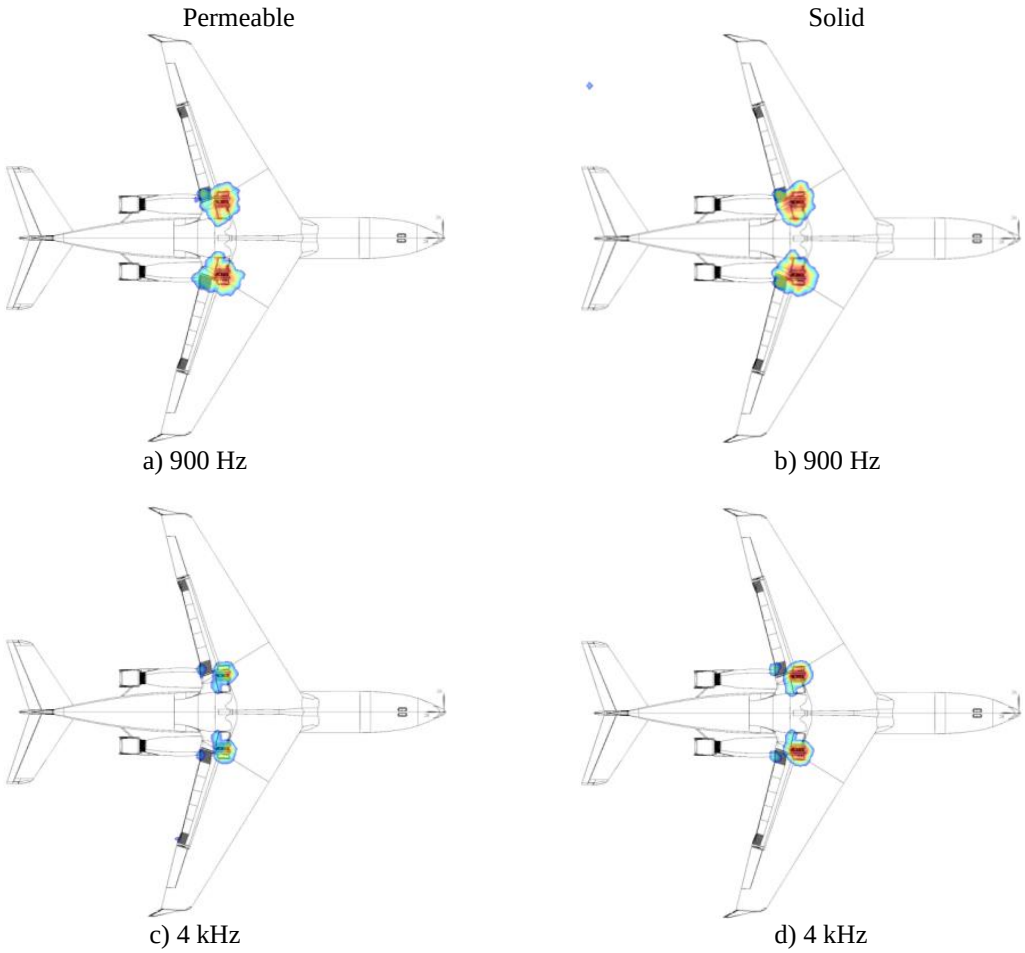

Fig. 13 1/12th octave CLEAN beamform maps from fine resolution simulations of G-III with ACTE flaps at moderate and high frequencies. Left column permeable surface and right column solid surface maps.

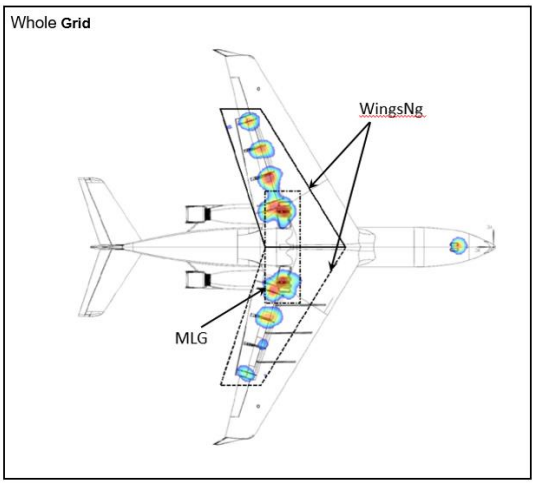

Fig. 14 Primary integration regions used for calculating integrated farfield noise spectra. Acoustic beamform map for 2.25 kHz is shown as an example (from Ref. [20]).

Integrated far-field spectra for the ACTE and Fowler flap configurations are shown in Fig. 15. Observe that, for these two G-III configurations, the spectra from the solid and permeable surfaces are in excellent agreement up to moderate frequencies close to 1 kHz. Above this frequency, the permeable data surface spectrum underpredicts the solid surface spectral levels, with the magnitude of underprediction increasing with frequency. Although a good portion of the underprediction can be attributed to diffusion (spatial resolution) effects within the volume enclosed by the permeable data surface, improper simulation of shielding effects (especially at high frequencies) by the solid surface formulation is, most likely, also a cause of the difference in noise levels. While the good agreement between flight test results and solid surface spectra from our finest resolution simulations, as observed in Fig. 15, gives reason for optimism, one must be cognizant of the fact that this agreement may be fortuitous. Unfortunately, the prohibitive computational resource and cost requirements of these simulations precluded efforts at higher spatial resolutions to determine whether a) the solid surface spectrum is fully converged at high frequencies, and b) the permeable surface spectrum approaches the solid spectrum levels at higher frequencies or shielding effects prevent the two spectra from ever collapsing.

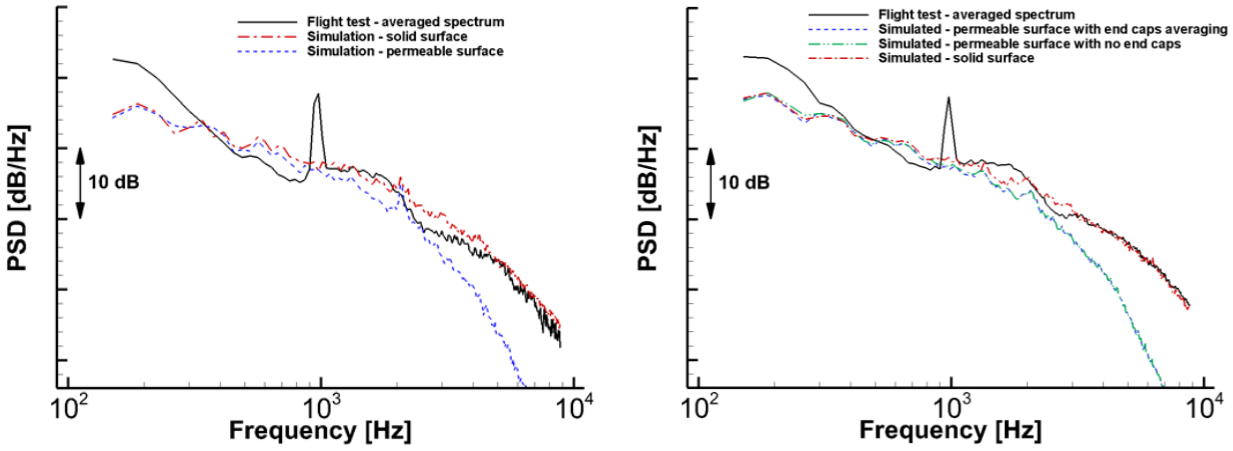

a) "MLG" region for G-III with ACTE flap

b) "WingsNg" region for G-III with Fowler flap

Fig. 15 Integrated far-field spectra for two G-III aircraft configurations (from Ref. [20]).

Once the NLG was included in the simulations of the G-III with Fowler flaps [21], familiar complications with the solid surface data approach arose. That is, similar trends to those for the isolated B777 NLG were observed for the G-III NLG, as seen in Fig. 16. Here, the effect is even more pronounced, with a sharp peak near 300Hz present in the solid results. As illustrated in Ref. [21], the origin of this tone was traced to a hydrodynamic, nonpropagating mode trapped inside the NLG cavity. Clearly, the solid surface formulation inappropriately treats the mode as a propagating

sound wave. Conversely, the corresponding permeable surface spectrum (Fig. 16) does not contain a tone near 300 Hz, corroborating the nonpropagating nature of this trapped mode.

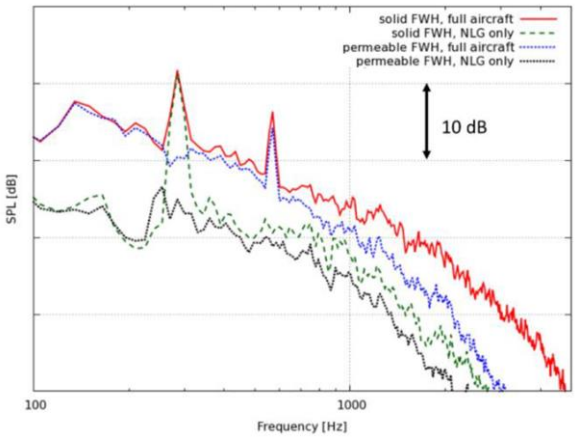

Fig. 16 G-III NLG comparison of solid and permeable surfaces (from Ref. [21]).

C. LCT

In light of the issues noted for the solid surface results of the 26% B777 MLG and full-scale, isolated NLG configurations, we relied exclusively on permeable surface data for predicting the far-field noise signature of the complete, full-scale 777 aircraft (see Ref. [23]). Hence, no LCT results are presented.

D. GLBC

The simulated, single-microphone, far-field noise data for the GLBC were augmented with results obtained from an 800-element synthetic phased microphone array placed underneath the aircraft, at 90° [28]. A smaller, 97-element synthetic array was placed above the model also, at 270°. These angles are given relative to the ground after accounting for convection effects. Although the second array does not provide significant insight into the airframe noise signature on the ground, it was employed mainly to investigate some of the deficiencies of solid surface data when shielding is present. The array-generated CLEAN beamform maps were integrated to extract component and total airframe noise spectra. Judiciously designed regions, shown in Fig. 17, were used to perform the integration and obtain the spectra in the overhead direction. The same grid and integration regions were also used to show the sources as seen by the array above the GLBC model.

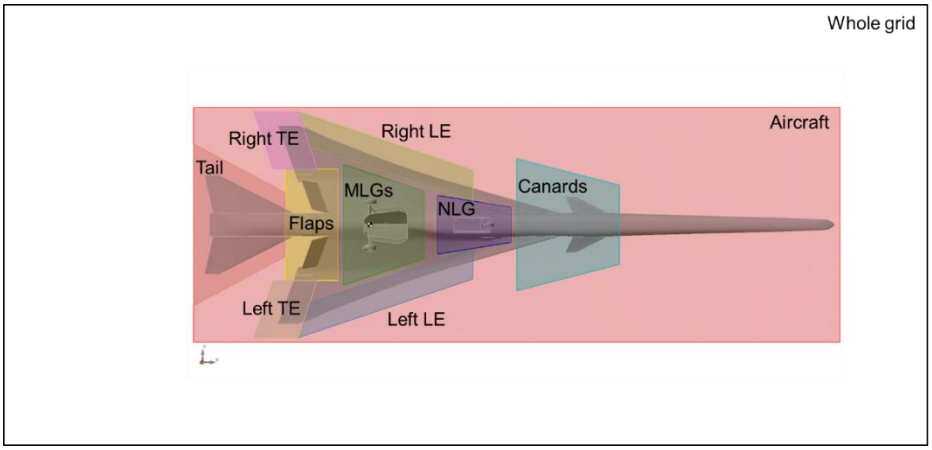

Fig. 17 Regions used to calculate integrated far-field noise spectra for GLBC (from Ref. [28]).

Sample CLEAN beamform maps for the GLBC model obtained from solid and permeable data surfaces are compared in Fig. 18 for the overhead (90°) position. These results are presented in narrowband using a frequency resolution of ~500 Hz in model-scale. Near 3.85 kHz (Fig. 18a), both data surfaces yield similar peak levels, with the MLG as the primary source of noise. However, the solid data surface formulation also shows the leading-edge vortices

to be prominent sources, as indicated by the high-SPL (red) regions near the wing tips (see Ref. [26] for an aerodynamic analysis of these flow structures). The permeable data surface formulation, on the other hand, captures shielding effects correctly – the weaker sources at the wing leading and trailing edges correspond to the noise generated by the vortices being scattered around the wing. Thus, for a ground observer, the sound would appear to emanate from the wing leading edge. A similar trend is observed at higher frequencies (Fig. 18b), where the vortex-induced noise sources that appear, erroneously, on the wing underside for the solid formulation become more dominant. Integrated spectra for the aircraft sources (obtained by adding the contribution from all individual components, e.g., canard, MLG, NLG, flaps, etc.), referred to as "Sum," are presented in Fig. 19. For completeness, results obtained from permeable data surfaces with and without end caps are also plotted in this figure. The inadequacy of the solid surface data is manifested as significant overprediction of spectral levels over the entire frequency range. As demonstrated in Ref. [28] for various airframe subcomponents, the excess levels stem from the noise sources on the GLBC upper surface that are shielded by the wing in the permeable data surface formulation.

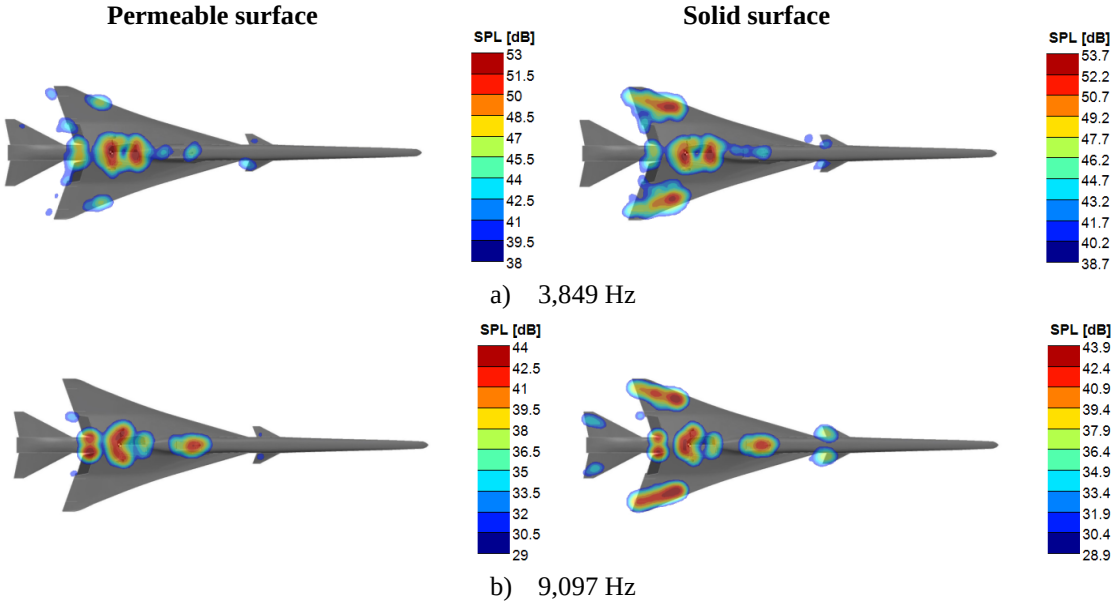

Fig. 18 Permeable vs. solid surface CLEAN maps for Flap30-LGon configuration (medium resolution [28]). Results from permeable surface without end caps.

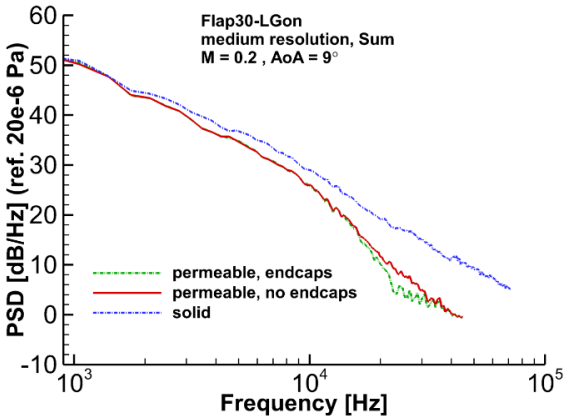

Fig. 19 Effect of data surface on integrated spectra for Flap30-LGon configuration (medium resolution [28]).

Although not included in Ref. [28], CLEAN maps obtained from the smaller, 97-element synthetic array placed above the GLBC confirmed the shielding issues encountered when solid surface data are used. A small subset of these maps is shown in Fig. 20 for model-scale frequencies of 4,899 Hz (low) and 9,097 Hz (moderate). The permeable surface maps, obtained without end caps, correctly depict the expected airframe noise sources when the configuration

is viewed from above (e.g., wing leading edges, flaps, canards). While the solid surface maps contain sources similar to those obtained from the permeable surface, they incorrectly show sources associated with the nose and main landing gear. In addition, the peak levels in the permeable surface maps are typically 1–2 dB higher than those for solid surface data at low and moderate frequencies. This difference in levels is clearly demonstrated in the single-microphone and integrated spectra shown in Fig. 21. For completeness, permeable data surface results obtained with end caps are also included. Note that, contrary to the trend observed in Fig. 19, the solid surface underpredicts the permeable surface spectral levels at frequencies below 8 kHz when observed from above the aircraft, even though the solid surface also contains erroneous (nose and main landing gear) sources. The causes of this behavior are not clear to us. In most instances, solid surface data yield higher spectral levels, particularly at higher frequencies, due to diffusion (spatial resolution) effects on the propagating waves before they reach the permeable surface, as can be seen in Fig. 21 at frequencies above 12 kHz. For the present simulations, the spatialtemporal resolution was sufficient to render negligible any diffusive effects in the low-to-moderate frequency range. Thus, the underprediction of spectral levels observed in this range is not well understood and requires further study.

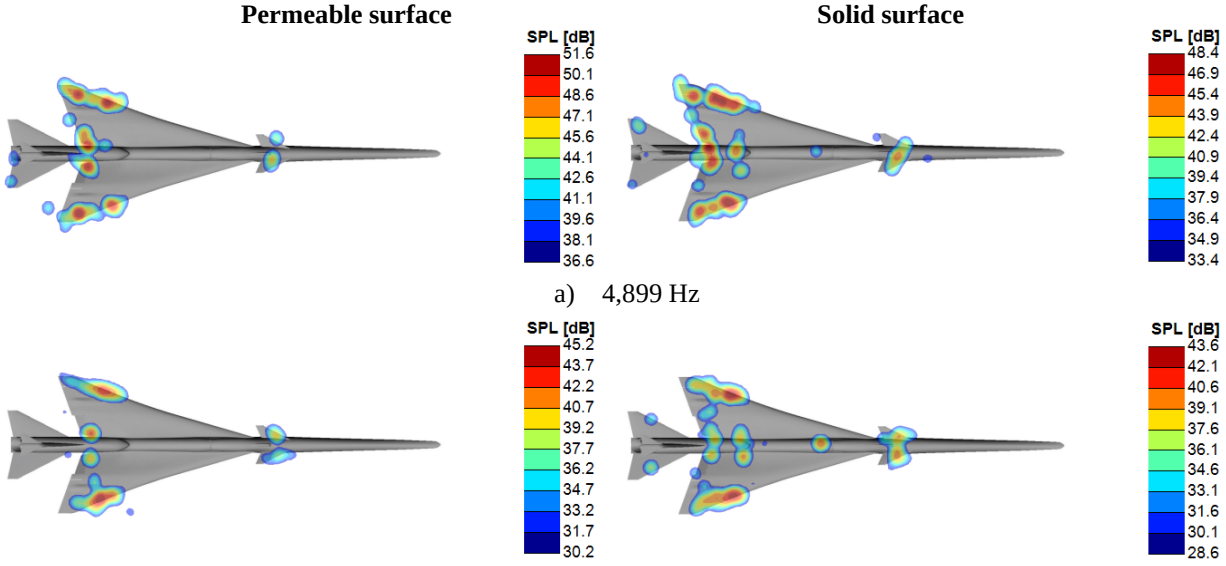

a) 4,899 Hz

b) 9,097 Hz

Fig. 20 CLEAN maps for Flap30-LGon configuration obtained from 97-element array placed above model (medium resolution). Results from permeable surface without end caps.

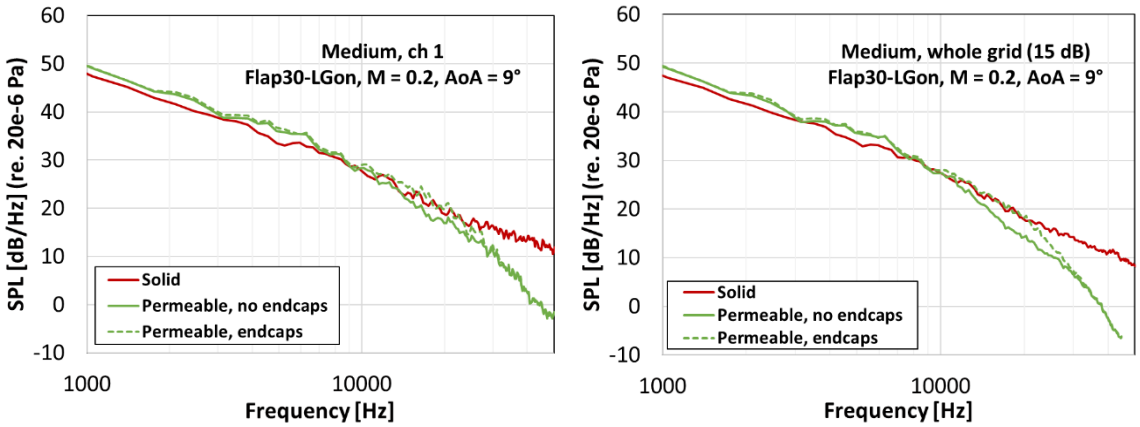

a) Array center (channel 1) microphone

b) Integration of "Whole" grid

Fig. 21 Effect of data surface on far-field spectra obtained from 97-element array above GLBC for Flap30-LGon configuration (medium resolution).

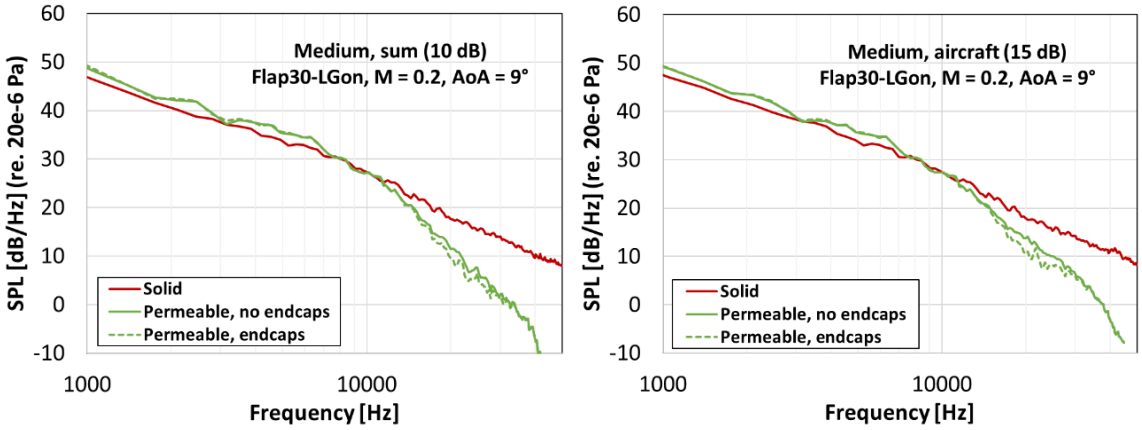

c) Integration of "Sum" of regions

d) Integration of "aircraft" region

Fig. 21 Concluded.

VI. Placement and Shape of Permeable Data Surfaces

Determination of the extent and position of permeable data surfaces is a nontrivial exercise, as these surfaces must balance computational cost and accuracy of the computed far-field spectra within the frequency range of interest. The challenges in placing permeable data surfaces far from hydrodynamic fluctuations without making a simulation too expensive or dissipating the pressure waves before they reach the data surfaces will be discussed in this section.

A. Isolated NLG

A permeable data surface deemed adequate, after some experimentation, for high spatial resolution simulations of the isolated NLG configuration is depicted in Fig. 22. The surface enclosed a volume with rectangular cross section and had seven end caps, as shown in Fig. 22a. Note from the figure that a "generous" width was associated with this surface. However, once significant differences between solid and permeable data surface noise levels emerged, attention was focused on the state of the NLG wake and its interaction with the permeable data surface. As displayed in Fig. 22b, scrutiny of the NLG wake revealed spillage of hydrodynamic flow fluctuations in the downstream segment of the surface through the side faces. To eliminate this anomaly, the rectangular surface width was carefully expanded in the downstream direction to include all flow fluctuations produced by the NLG and highlighted in Fig. 7 as the isosurface of 1% standard deviation of velocity magnitude fluctuations. As demonstrated in Ref. [24], the resulting permeable data surface was optimized such that the predicted far-field noise spectrum was in excellent agreement with QTD2 flight test acoustic measurements.

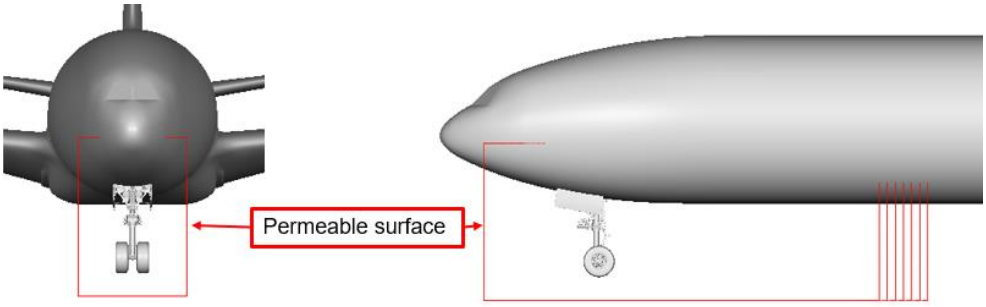

a) Initial permeable surface

Fig. 22 Shape and extent of initial permeable data surface for isolated B777 NLG.

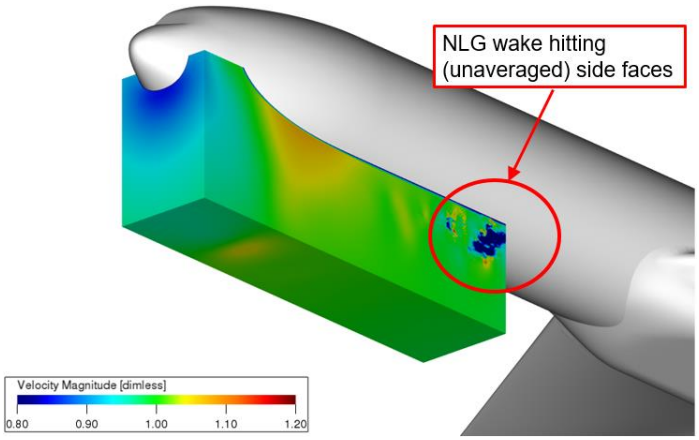

b) Contours of instantaneous velocity magnitude on permeable surface faces

Fig. 22 Concluded.

B. G-III

The most efficient location for a permeable data surface is a trade-off – not too close to the aircraft as to pollute the results with near-body hydrodynamic effects, while at the same time close enough as to not incur unnecessary simulation cost with the desired resolution considerations. Attempts were made early during aerodynamic simulations of the G-III ACTE geometry to understand the effects the extent of the enclosed volume and end cap placement had on the resulting spectra, taken at single microphone locations along the centerline of the aircraft. Two separate coarse-resolution simulations, each fitted with a different permeable data surface, were completed to gain further understanding of end cap effects and permeable surface placement. During these early studies, the extent of the permeable surface and the number and orientation of the surface end caps were examined in a relatively coupled fashion. The results presented in this section reflect that approach. Data from a study targeting the effects of end caps on noise source distribution and far-field spectra are presented and discussed in Section VII.B.

Fig. 23 shows the two permeable surfaces considered during the G-III-ACTE study. The surface labeled "Vertical" was created such that any streamwise vortices or large flow structures generated by the airframe would exit the data surface as normal to each end cap as possible, with minor inherent variations to account for angles of attack representative of landing conditions. The surface labeled "Tilted" was created to gain the benefit of employing end caps while minimizing the extent of the total volume resolved. In this figure, the end caps shown in the aircraft image were averaged to produce the plotted spectra. For frequencies below 2 kHz, the tilted permeable surface produced levels that were generally about 1 dB higher than those from the vertical permeable surface. Higher frequencies show less sensitivity to the tilted surface, meaning that the end caps are likely less affected by smaller flow structures.

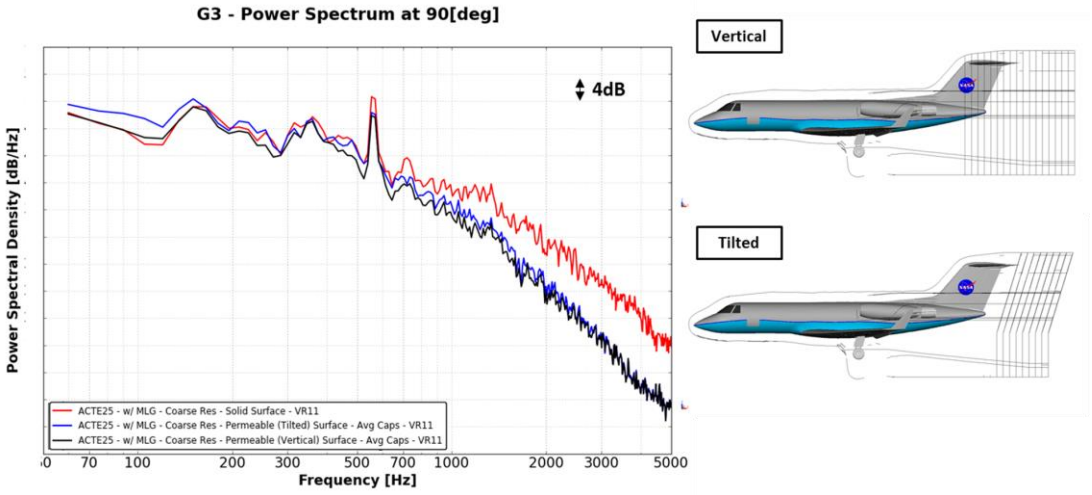

Fig. 23 Effect of varying permeable surface shape on a single overhead microphone from G-III ACTE aircraft simulation data.

The surface with the tilted end caps was used as the baseline to examine further the effects on far-field noise when the extent of the permeable surface or the location of the end caps in the "Vertical" surface are modified. Some of the prominent changes studied are displayed in Fig. 24. The image in Fig. 24a shows the end caps repositioned such that they intersect the empennage and terminate at the elevator's trailing edge. The image in Fig. 24b shows only those end caps that existed downstream of the aircraft surface. The impact of end cap spacing on far-field noise was evaluated by doubling the original 0.5 m spacing between successive caps to 1 m, as shown in Fig. 24c. All surface and end cap modifications displayed in Fig. 24 produced negligible differences relative to the spectrum associated with the original Vertical surface presented in Fig. 23.

a) End caps intersecting aircraft b) End caps not intersecting aircraft c) End cap spacing doubled

Fig. 24 Modified surface, end cap position, and end cap spacing used for G-III ACTE aircraft simulation.

Fig. 25 depicts the effect on spectra from the overhead microphone location when the aft end of the permeable surface is terminated at varying streamwise locations. The EC01 (blue line) data correspond to a permeable data surface extending up to, and including, the first end cap only. The EC17 (black line) data represent the result of a permeable surface extending up to, and including, the location of the last end cap. Any end caps upstream of this last flow-normal face were excluded from the permeable surface measurement data to generate the spectrum. Thus, we were able to assess the effect of including (thereby resolving) more volume downstream of the aircraft in our permeable surface measurement. Note from the figure that little difference exists between the resulting spectra in the frequency range considered to be resolved by the simulation.

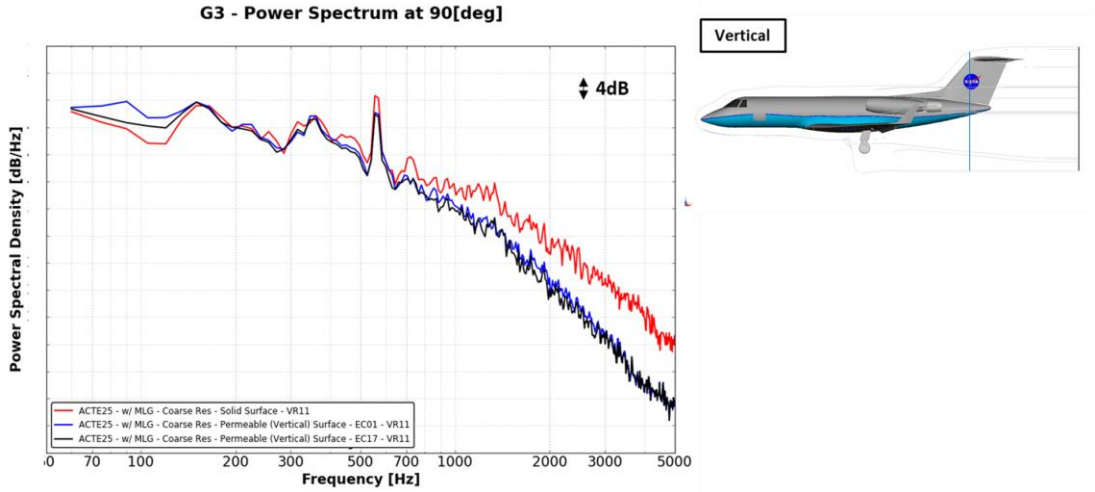

Fig. 25 Effect of varying resolved volume within a permeable surface on a single overhead microphone from G-III ACTE aircraft simulation data.

The study undertaken to quantify the effects of end cap placement and permeable surface shape on the G-III ACTE simulation data was an attempt to place the permeable surface more efficiently for finer resolution simulations, thus reducing expense while minimizing the impact on the results. As mentioned in Section V.B, ultimately the reduced permeable surface shown in Fig. 12 was utilized for both G-III configurations to facilitate execution of the simulations at the highest possible spatial resolution. The results from the various studies shown in this section, while important, are specific to a particular set of geometry and flow conditions. Ultimately, the highest benefit of end cap usage and their placement in a permeable data surface will be realized when there are strong, coherent flow structures which may otherwise pollute the measurements on the surface. The general lack of variation among permeable surface results sampled from the G-III with ACTE flaps is indicative of both a lack of strong pressure fluctuations in the wake

generated by this aircraft configuration and the effect of various end cap arrangements. If this study were performed on an aircraft equipped with traditional Fowler flaps and their associated side edges, gaps, tracks, and other retracting mechanisms, or on one generating a more complex flow field (as will be seen in section VII.B), then the effect of end caps would likely be more evident. Thus, the main conclusions of this study are: 1) a thorough understanding of the flow field generated by the aircraft is paramount to fitting the most efficient permeable data surface, as there is no one-size fits all answer, and 2) if the flow field does not contain strong, coherent structures that convect downstream from the aircraft, the expense of wrapping voluminous permeable surfaces around the configuration can be avoided.

C. LCT

For the LCT studies, the nominal permeable data surface was designed using the cruise wing configuration (Config1) with nose and main landing gear deployed and high-lift devices retracted. As shown in Fig. 26, a generous portion of the volume underneath the wing was included in the Config1 permeable data surface, anticipating that such a surface would be sufficient to encompass the landing configuration (Config2) where slats and flaps are fully deflected. Despite our best effort, the increased downwash that resulted from deployment of high-lift devices in Config2 changed the wake position substantially, causing the peripheral part of the wake to spill out of the Config1 surface. The sample CLEAN map in Fig. 27a clearly shows the artifacts of hydrodynamic fluctuations (numerical sources) exiting the lower portion of the surface in the inboard segment of the wing. As a case study, the permeable surface underneath the wing was extended downward to contain the flap and MLG wake. The additional volume enclosed by the larger permeable data surface for the high-lift wing (Config2) required refinement to avoid numerical diffusion of high-frequency noise prior to reaching the data surface. This seemingly minor modification of the initial permeable surface increased the grid size by about 6%, which for the "coarse" resolution case amounted to 1 billion additional volume elements or voxels. The corresponding beamform map obtained from the Config2 surface is shown in Fig. 27b. Notice the disappearance of the unphysical sources in the wake for the enlarged surface. As demonstrated in Ref. [23], through judicious selection of integration regions (see Fig. 28), the beamform maps from Config1 can be salvaged to eliminate the numerical noise sources and extract the correct far-field noise spectrum. Shown in Fig. 29 are spectra obtained from integration of the entire beamform plane (Whole Grid) vs. the "Sum" of contributions from integration of subregions defined in Fig. 28 (see Ref. [23]). Note from the figure that, as anticipated for the Config1 (nominal) surface, the contribution from numerical sources to the far-field spectrum can be determined when integrated results from the "Whole Grid" are compared to those from the "Sum" of subregions – the numerical noise is manifested as an excess for frequencies above 2 kHz. In contrast, the spectra obtained from the expanded (Config2) surface, regardless of whether the "Whole Grid" region or the "Sum" of subregions was used to perform the integration, are similar. More importantly, note also that the "Sum" of contributions from the integration subregions defined in Fig. 28 is nearly identical between the nominal and expanded permeable data surfaces. This observation reinforces the fact that, with carefully chosen integration regions, the contribution of unphysical noise sources can be excluded from far-field spectra. Abundantly clear here is the fact that, without application of phased microphone array analysis, the identification of numerical noise sources and removal of their contribution to the far-field noise spectrum would have been almost impossible.

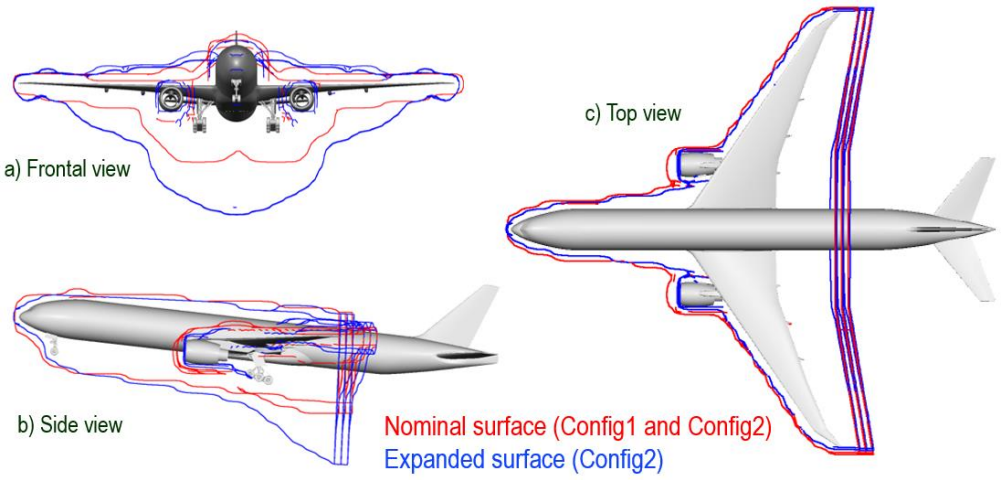

Fig. 26 LCT permeable data surfaces for Config1 (nominal, red line) and Config2 (blue line) used for far-field noise computations (from Ref. [23]).

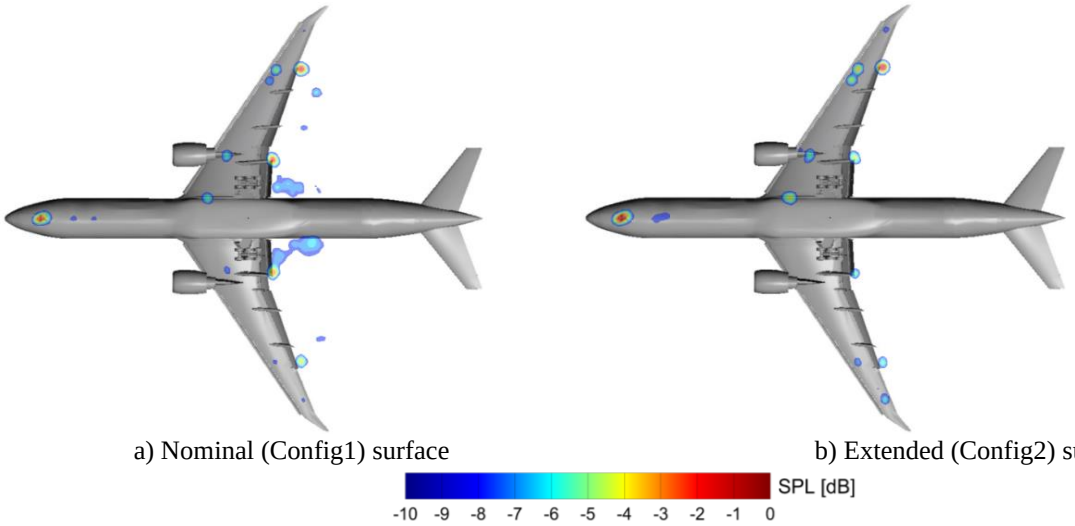

a) Nominal (Config1) surface b) Extended (Config2) surface

Fig. 27 CLEAN maps showing effect of permeable surface extent for Config2 at 2.65 kHz (from Ref. [23]).

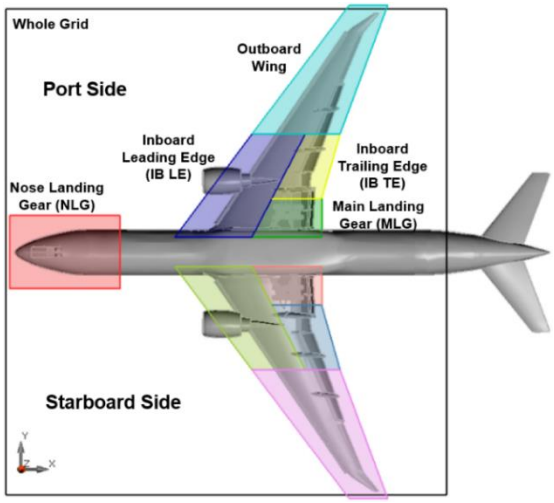

Fig. 28 Tailored regions used to calculate integrated far-field noise spectra for various components and full aircraft (from Ref. [23]).

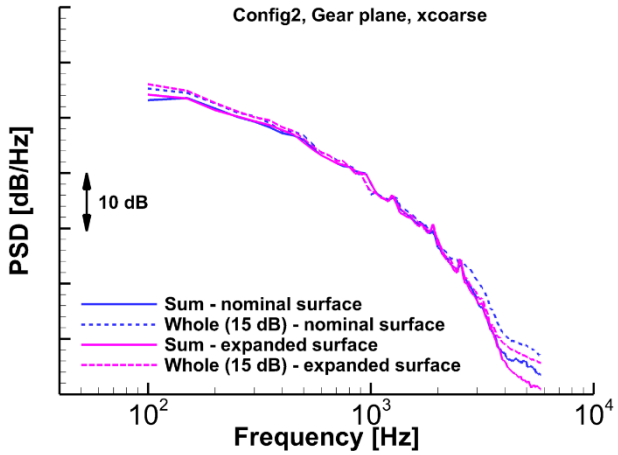

Fig. 29 Influence of integration region and permeable data surface extent on the far-field noise spectrum of Config2 (from Ref. [23]).

D. GLBC

The flow field generated by the GLBC imposed new challenges on the development of an appropriate FW-H permeable data surface that are unique to supersonic aircraft. As shown in Fig. 30, the flow over the wing is characterized by a multitude of streamwise vortices of various spatial and temporal scales that separate from the surface and meander substantially. Thus, a proper permeable data surface had to meet two criteria: 1) be sufficiently extensive on the underside of the aircraft to contain the flow fluctuations associated with the landing gear and deflected flaps; and 2) include a substantial volume on the upper side of the aircraft to encompass the detached, meandering vortices. As shown in Fig. 31, the chosen permeable surface with five endcaps covered a substantial volume in the GLBC wake and the upper side of the model. Care was exercised to position all five caps within the same fine variable resolution region. Mesh resolution was lowered downstream of the last endcap. Although these endcaps should be placed as far downstream as possible, the computational cost of such a choice must be considered always. For the GLBC and cruise LCT, the cells used to propagate pressure fluctuations to the permeable data surface represented 10% and 30% of the total computational mesh, respectively.

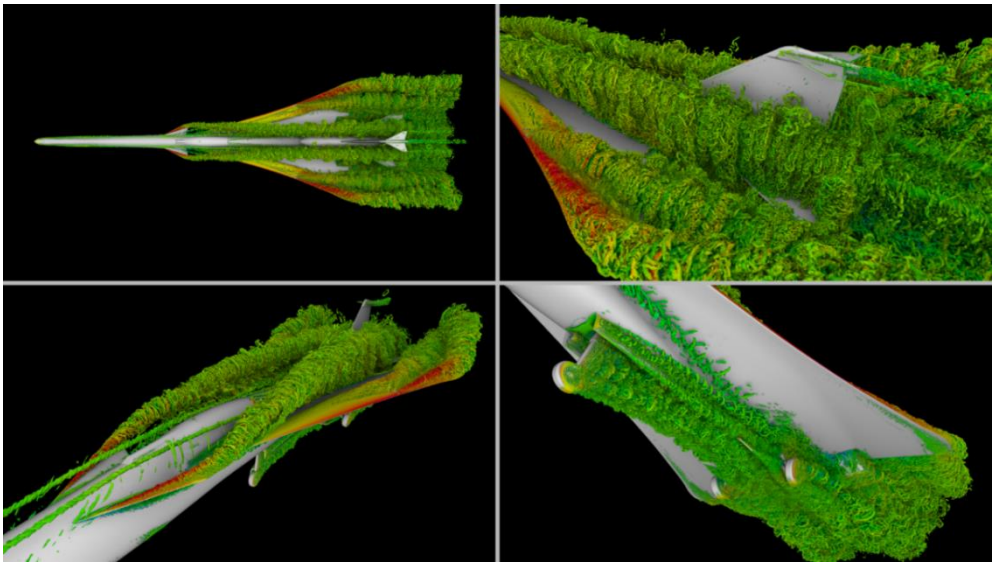

Fig. 30 Instantaneous vorticity field based on isosurfaces of λ_2 criterion for the GLBC model in landing configuration (Flap30-LGon). Results from free-air, fine spatial resolution simulation at AoA = 9°.

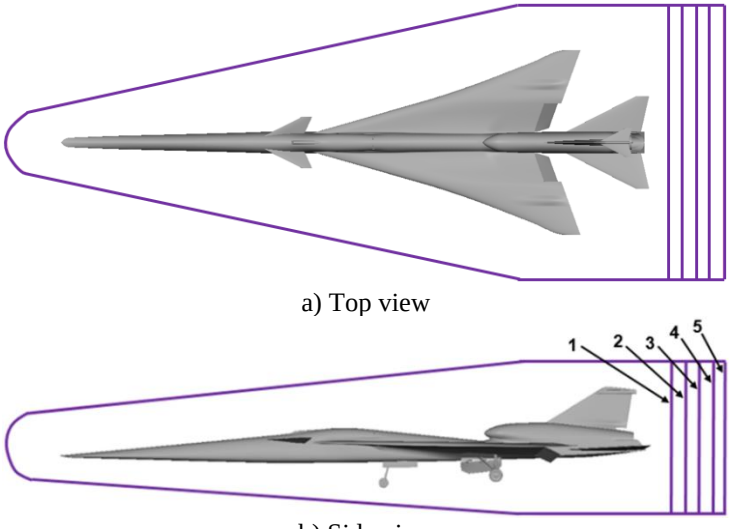

a) Top view

b) Side view

Fig. 31 GLBC model with permeable FW-H data surface drawn in purple lines [27]: (a) top and (b) side views.

VII. End Cap Effects

Spurious (numerical) noise may be created when hydrodynamic fluctuations cross a closed permeable data surface. However, avoiding all such intersections is impossible in the presence of wakes. A potential avenue to circumvent this issue is to open the surface by removing the segment downstream of the aircraft. Aside from theoretical ramifications, a disadvantage of open data surfaces is that they are inaccurate for microphones at shallow directivity angles, i.e., significantly forward or aft of the aircraft. A common and simple approach to diminish significantly the impact of hydrodynamic fluctuations in wakes exiting a permeable data surface is to perform end cap averaging (see Fig. 31), which is equivalent to averaging the results of several closed permeable data surfaces. In this section, we highlight issues encountered in our studies with end cap averaging.

A. Isolated NLG

As depicted in Fig. 7, for the isolated NLG setup, seven end caps at the downstream segment of the permeable data surface were used to diminish, through averaging, the effects on far-field noise caused by hydrodynamic flow fluctuations leaving the permeable surface. The spectra obtained from using no caps (open surface at the downstream side), one cap, and the average of all seven caps are shown in Fig. 32. The spectra are almost identical, suggesting that for the NLG configuration, neither the permeable surface exit plane nor the number of caps influence the noise spectrum. The single-probe power spectral density (PSD) results of Fig. 32 were corroborated by the synthetic microphone array results of Ref. [25]. A sample conventional beamform map obtained from fine resolution, averaged-cap permeable data are presented in Fig. 33. The rectangular area enclosed by the black line called "Whole Grid" depicts the extent of the beamform plane that contains the NLG permeable surface, including its seven end caps. The map does not show any numerical (unphysical) sources that typically appear at the downstream boundary of the data surface. Notice that for these maps, a 15 dB cutoff range was used to ensure inclusion of weaker sources. We can conjecture plausible reasons for this lack of dependency of the noise spectrum on the conditions at the exit plane. First, the exit plane for our chosen surface may be far enough downstream to allow the hydrodynamic flow fluctuations to diffuse sufficiently and decorrelate prior to leaving the permeable surface. Unfortunately, we did not experiment with the downstream position of the exit plane to determine if moving it forward would adversely affect the levels or the content of the far-field noise signature. Second, the dynamics and evolution of the flow structures produced by the various bluff bodies of the NLG may be quite different than those of longitudinal vortices. As will be shown in later examples, unphysical sources appear at the permeable surface segments where strong streamwise vortices, such as those produced at the wing or flaps tips, pass through the surface. Obviously, such vortices possess high spatio-temporal coherence and thus behave differently than the turbulent wake of a landing gear. However, as demonstrated clearly in Ref. [24], the far-field noise spectrum obtained with the present permeable surface for the isolated NLG is in excellent agreement with QTD2 flight test measurements, validating the appropriateness of the simulation set-up.

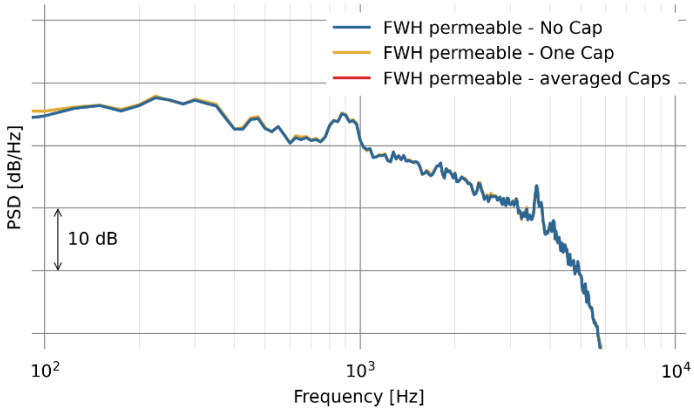

Fig. 32 Single-microphone PSD plots demonstrating influence of end caps on near-field noise spectrum.

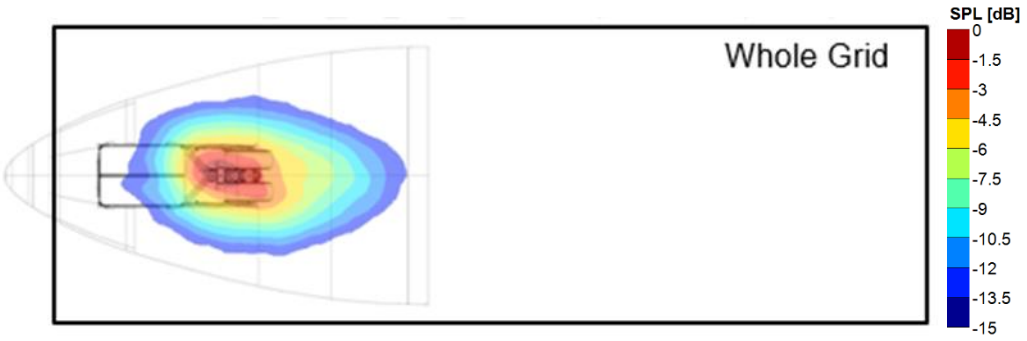

Fig. 33 Conventional 1/12th octave beamform map at 2.5 kHz from fine resolution permeable surface data for isolated NLG configuration. A cutoff range of 15 dB was used to show potential weaker sources.

B. G-III

The permeable data surface depicted in Fig. 12 was ultimately used to conduct our finest resolution simulations. The influence of the permeable surface exit plane on the G-III farfield noise signature was examined carefully. Sample 1/12th octave CLEAN beamform maps at 900 Hz for the configuration with Fowler flaps are shown in Fig. 34. The maps, created with a cutoff range of 10 dB, were generated from synthetic array pressure records sampled at a data surface with end cap averaging and without end caps (open surface). The map associated with end cap averaging shows the presence of relatively weak numerical sources downstream of the wing trailing edge, at the location where flow structures within the flap wake pass through the exit plane of the permeable data surface. In contrast, such unphysical (numerical) sources are absent in the map produced from the data with no end caps, or they may reside below the 10 dB cutoff range. To explore this issue further, the synthetic pressure records were processed with a 15 dB cutoff range and the resulting maps are shown in Fig. 35. Notice that with this higher cutoff threshold, extremely weak numerical sources now appear in the wake region of the map without end caps. However, given their relatively low levels, these sources would have no impact on the far-field noise levels. Scrutiny of the CLEAN maps over the entire frequency range of interest revealed that numerical sources appear on the exit face of the data surface only within the 700 Hz to 1.25 kHz frequency range.

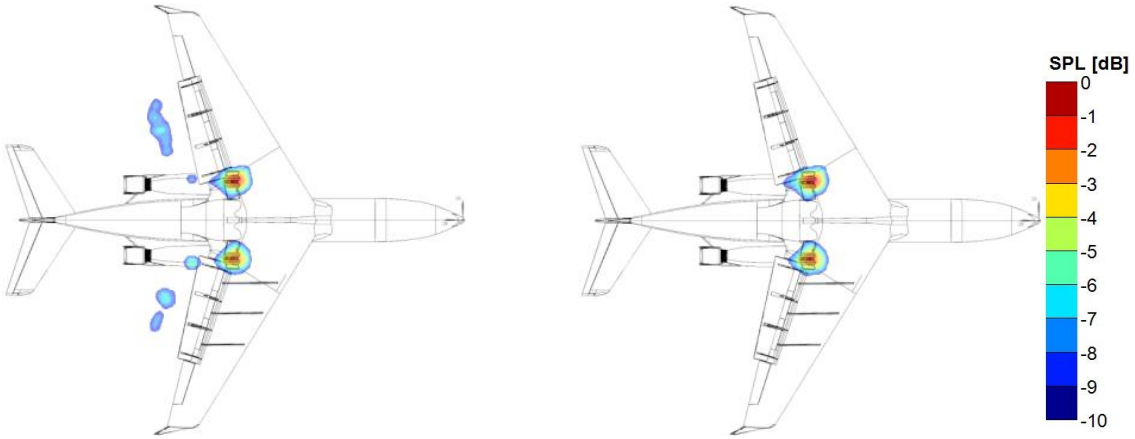

a) Averaged end caps b) Without end caps

Fig. 34 1/12th octave (900 Hz) CLEAN maps for G-III, 10 dB cutoff.

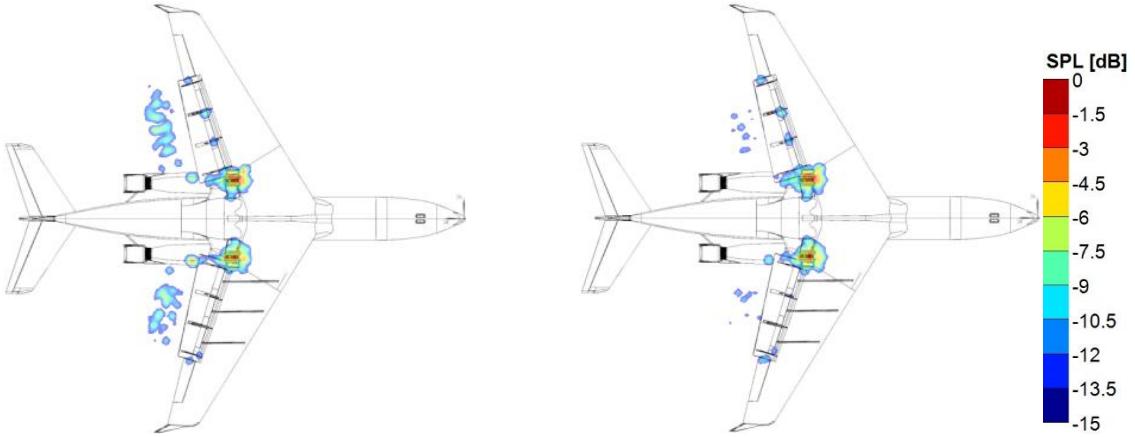

a) Averaged end caps b) Without end caps

Fig. 35 1/12th octave (900 Hz) CLEAN maps for G-III, 15 dB cutoff.

To determine the contribution of numerical sources at the exit plane to the far-field noise spectrum, integration of the entire beamform plane "Whole Grid", as well as the "WingsNg" region, was performed. Resulting spectra from the averaged caps and no end cap data are presented in Fig. 36a. As examination of the beamform maps revealed, numerical noise appears in the spectrum obtained from the end cap averaged permeable surface data in the frequency range of 700 Hz to 1.25 kHz. Notice that the corresponding spectrum obtained from integration of the WingsNg region is almost identical to the spectra obtained from the no-cap permeable surface data, regardless of the region used to perform the integration. The contribution of the sources at the exit plane can be corroborated independently by examining the average of all spectra from the array microphones. This averaged spectrum is a good representation of the total array output. The array-averaged spectra obtained from the permeable surface data with averaged end caps and no end caps are shown in Fig. 36b. As expected, these noise signatures follow the same trends as those obtained from integration of the beamform maps shown in Fig. 36a. Again, the results shown in Fig. 36 corroborate our assertion that, with judicious tailoring of integration regions, in most instances one can successfully eliminate numerical source contributions to far-field noise. Note, however, that such a procedure implies the use of microphone array processing techniques and a careful analysis of the resulting beamform maps, which substantially increase the cost of any airframe noise study.

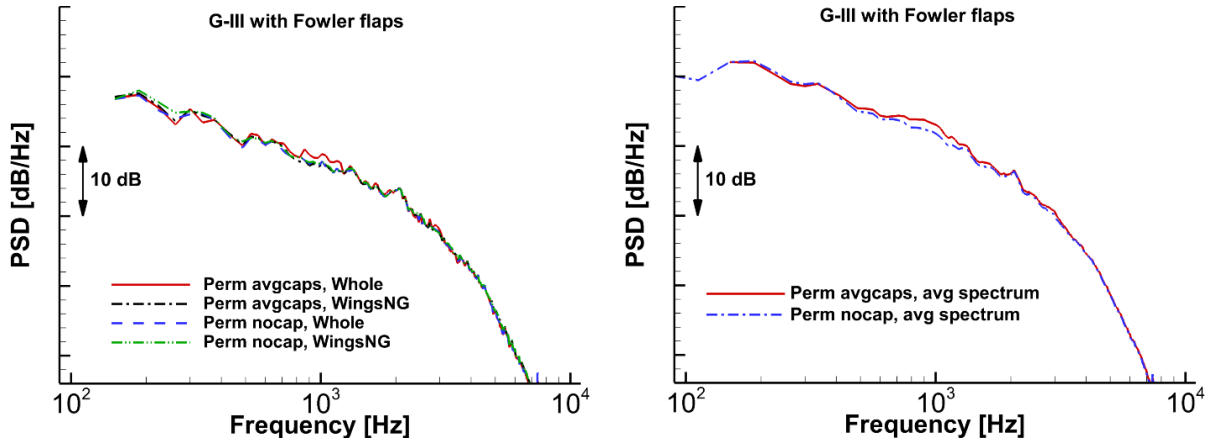

a) Integrated spectra b) Array-averaged spectra

Fig. 36 Comparison of integrated and array-averaged spectra obtained from permeable surface data with end cap averaging and no endcap. Data from simulation of G-III configuration with Fowler flaps.

C. LCT

An in-depth study of end cap effects was not conducted for the LCT, as the insights gained from the isolated NLG and G-III investigations were deemed applicable to this configuration as well.

D. GLBC

During preliminary assessment of GLBC data simulated with the 5-end-cap surface depicted in Fig. 31, single-microphone spectra corresponding to the array centerline were used to evaluate convergence of the predicted noise with increasing spatial resolution. Comparison of the spectra at three resolution levels showed rapid convergence of the far-field spectrum up to frequencies of 25 kHz to 30 kHz model-scale, as seen in Fig. 37. As discussed below, this behavior was erroneous since the high-frequency segment of the spectrum was heavily influenced by numerical sources generated by the passage of streamwise vortices through the end cap region. In other words, the single-microphone data were depicting convergence of high-frequency numerical sources. That initial observation was discarded once the synthetic array pressure data were processed. Sample CLEAN maps presented in Fig. 38 show the GLBC noise sources at moderate and relatively high frequencies. Notice that at lower and moderate frequencies, the maps are dominated by typical airframe sources (e.g., main and nose landing gear, flaps) that mask partially the presence of, and contribution from, numerical sources at the end caps. However, with the reduction in strength of the primary airframe sources at higher frequencies, the numerical sources at the end caps dominate the spectra and their contribution effectively masks the noise levels associated with the true airframe sources. As demonstrated in Ref. [28], numerical source contribution to the far-field spectra is manifested over the entire frequency range of interest when the clean (cruise) configuration of the GLBC is examined. For airframe noise studies, the clean configuration typically represents the quietest aircraft configuration and serves as a baseline for the assessment of noise from high-lift devices or landing gear.

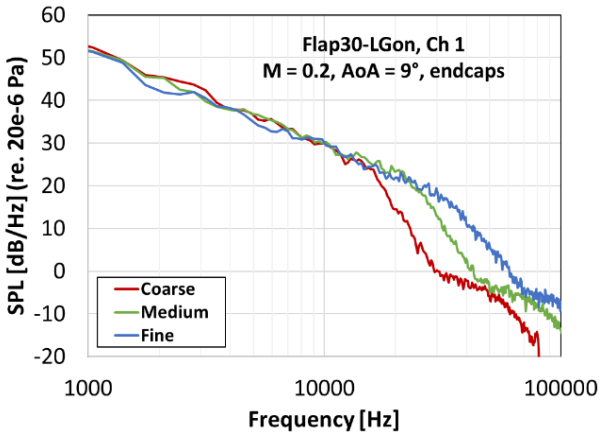

Fig. 37 Spatial resolution effects on spectra of Flap30-LGon (landing) configuration with end caps, array center microphone.

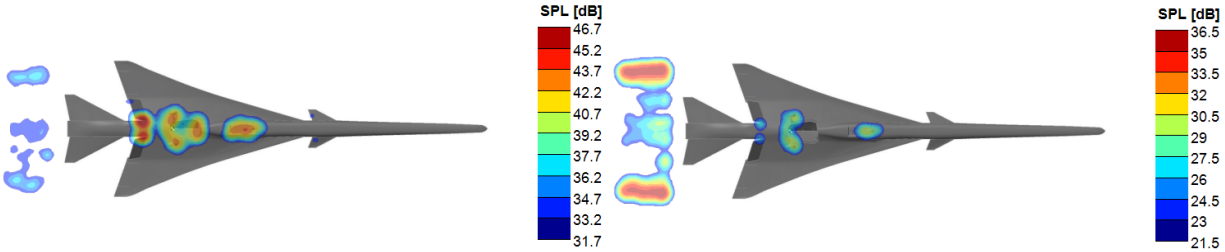

a) 7,698 Hz b) 17,845 Hz

Fig. 38 Effect of end caps on CLEAN maps from medium resolution simulation of Flap30-LGon (landing) configuration [28]: (a) 7,698 Hz and (b) 17,845 Hz, in narrowband with ~500 Hz resolution.

An extensive study to determine the effects of end cap number and spacing on far-field noise was undertaken. Results from this study are presented in Fig. 39. In Fig. 39a, we show far-field spectra from the array center microphone (channel 1) for cases considering all five end caps (red line); end caps 1, 3, and 5 (green line); end caps 3, 4, and 5 (blue line); end cap 5 (black line); and no end caps (orange line). Corresponding spectra obtained from integrating CLEAN maps (with a 15 dB cutoff) for the "Whole" grid (see Fig. 17) that covers the entire scanning plane are shown in Fig. 39b. Notice that integration of this region yields spectra very similar to those of the single-microphone, indicating that the array has captured contributions from all simulated noise sources, physical and

numerical. Observe from Fig. 39a and Fig. 39b that a single end cap produces the highest noise levels, particularly at higher frequencies. In contrast, the spectrum obtained with no end caps shows the lowest noise levels. By adding more end caps, the spectral levels drop and approach those obtained without end caps. Clearly, convergence is slow and no reasonable number of end caps will fully mitigate the contribution of numerical sources generated at the exit plane. Comparison of spectra in Fig. 39a and Fig. 39b obtained with end caps 1, 3, 5 and 3, 4, 5 reveals that doubling the distance between successive end caps does not affect the computed spectrum, but the number of end caps does. Obviously, this observation is based only on two spacings and a small number of end caps. Additional explorations are needed to arrive at more definitive trends and conclusions. The contributions from all subregions were added (based on p^2) to extract the total ("Sum") airframe noise produced by the physical (true) sources on the GLBC. A cutoff of 10 dB from the peak level in each subregion was used to perform the integration. The integrated spectra produced by this summation are shown in Fig. 39c. The same spectra were produced from integration of the "Aircraft" region (Fig. 39d), confirming that the subregions contained the total airframe noise for the GLBC. In Fig. 39c, notice that, regardless of the number of end caps used, the spectra are very similar for frequencies up to 16 kHz. The spatial resolution used in the simulation affects the accuracy of the computed levels at higher frequencies. The results clearly demonstrate that the numerical sources produced at the end caps do not contaminate the noise at other locations on the beamform maps, and that far-field spectra can be determined accurately through a judicious selection of integration regions. In addition, the single-channel spectrum computed without end caps provides the most accurate noise levels [28]. Possible theoretical violations and other ramifications of open FW-H permeable data surfaces were not considered. A clear example would be noise prediction at very low or very high directivity angles in the flyover direction, such as 0°-30° and 150°-180°, where contributions from the missing surface may be important. As indicated in Ref. [28], once the results obtained without end caps were deemed most accurate, this permeable data surface setup was used in all subsequent studies.

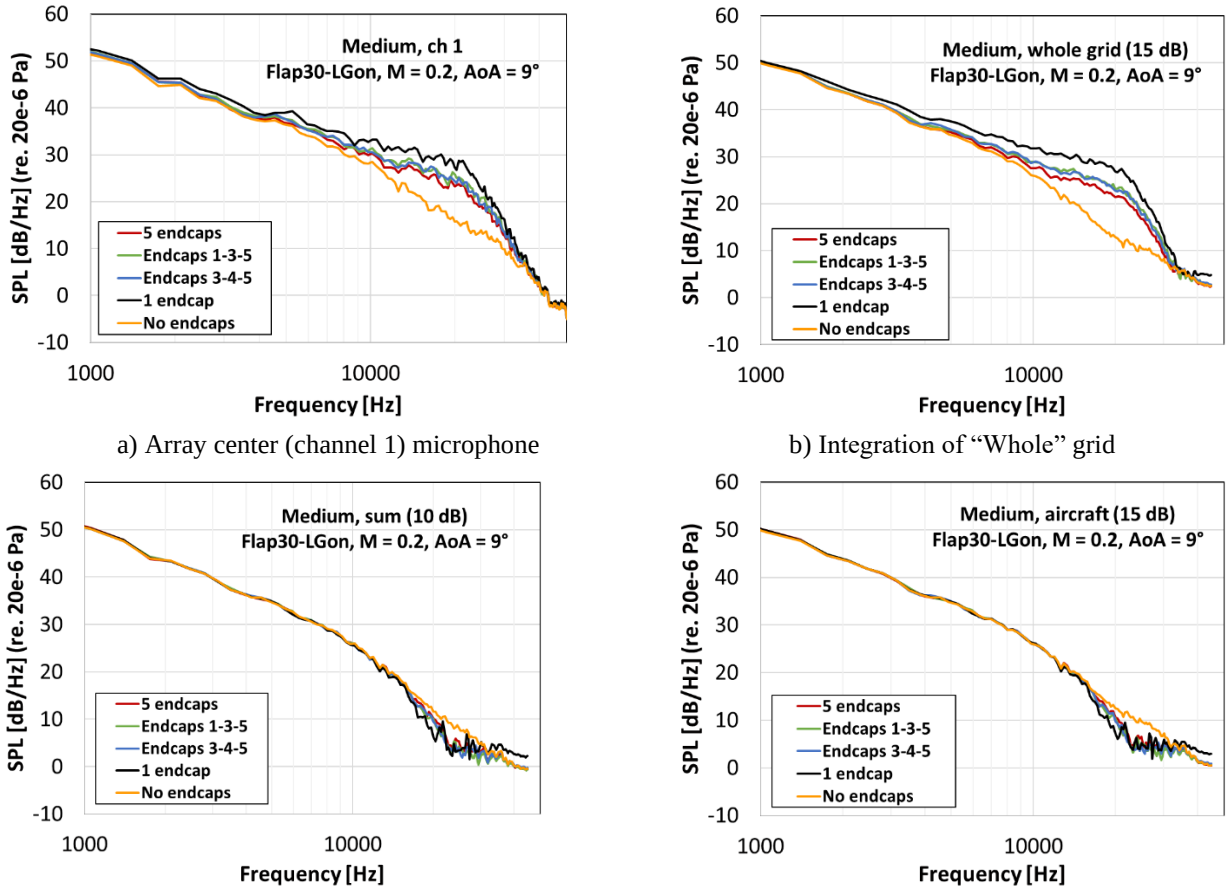

a) Array center (channel 1) microphone

b) Integration of "Whole" grid

c) Integration of "Sum" regions

d) Integration of "aircraft" region

Fig. 39 End cap effect on spectra obtained from medium simulation of Flap30-LGon configuration at overhead position.

VIII. Recommendations for the Use of Data Surfaces

Based on the examples shown in this paper, several recommendations or "desirable practices" can be made regarding the use of data surfaces for airframe noise propagation by means of the FW-H process. These practices are summarized in this section.

Permeable data surfaces should be preferred over solid data surfaces. The solid surface approach, although very attractive because of its simplicity and lower computational cost, has a high potential to introduce significant inaccuracies due to exclusion of flow nonlinearities, nonuniformities, and shielding effects. In general, the use of solid data surfaces can affect the noise levels substantially. When using permeable data surfaces, the enclosed volumes should be large enough to contain hydrodynamic fluctuations in wakes, but small enough to avoid excessive diffusion of pressure waves from the bodies to the data surfaces. Recall, for example, that on the GLBC, the top segment of the FW-H data surface was far enough from the wing to avoid intersecting the leading-edge vortices. On the LCT with flaps deployed, the bottom boundary of the permeable data surface was moved away from the aircraft to avoid contact with the wakes in the downwash.

The use of end caps may be unavoidable if the main receiver (microphone) locations are at significantly forward or aft directivity angles. In those cases, several caps should be included and used for averaging purposes. The possible presence of spurious noise caused by wakes crossing the end caps can be mitigated by increasing the number of end caps, as long as strong, coherent, vortical structures are not present. However, the benefits of using more than five to seven caps may not outweigh the associated high computational cost. In the presence of strong vortices, in particular streamwise vortices, the use of end caps is not recommended. If end caps are used, their associated spurious noise must be eliminated from the spectral levels. For a moderate range of flyover directivity angles including overhead, open data surfaces provide sufficiently accurate results.

FW-H results should be validated with directly measured synthetic data. This can be done by extending the fine spatial resolution region in the directions of interest beyond the permeable data surface and extracting the pressure fluctuations at those locations directly from the simulation. Extension of the fine resolution region will obviously impact the simulation cost, but the benefit of having these data cannot be overstated.

Proper noise source identification is critical. Understanding the nature of the acoustic sources is facilitated by the use of synthetic phased microphone arrays. We showed in this paper that "false positives" of spectral convergence can occur when spurious noise sources are present. This numerical noise affects grid convergence behavior by masking the strength of physical sources. Phased microphone arrays have become an indispensable and excellent tool to quantitatively differentiate noise sources and to remove regions where numerical noise is dominant. However, a large number of microphones significantly increases the computational cost of the noise propagation calculation, while beamforming adds complexity to the processing and analysis of acoustic data. Nevertheless, the benefits of these steps are substantial.

Acknowledgments

The present effort used data from numerous computational campaigns conducted under the Environmentally Responsible Aviation, Flight Demonstration and Capabilities, and Commercial Supersonic Technology projects of NASA. The authors gratefully acknowledge the invaluable contribution of Scott Brynildsen of Craig Technologies for providing geometry work, modifications, and CAD support for all simulations. We would also like to express our sincere appreciation for the support given by Patrick Moran, of the NASA Ames Research Center, for high-quality visualizations and animations of the large computational data sets. All simulations were performed on the computer clusters at the NASA Advanced Supercomputing (NAS) facility at the Ames Research Center. The logistical support provided by NAS staff, in particular Yan-tyng (Sherry) Chang, is greatly appreciated.

References

[1] M. R. Khorrami and E. Fares, "Toward noise certification during design: airframe noise simulations for full-scale, complete aircraft," *CEAS Aeronautical Journal,* vol. 10, pp. 31-67, 2019.

[2] J. E. Hawkings and D. L. Ffowcs Williams, "Sound Generation by Turbulence and Surfaces in Arbitrary Motion," *Philosophical Transactions of the Royal Society of London. Series A, Mathematical and Physical Sciences,* vol. 264, no. 1151, pp. 321-342, 1969.

[3] F. Succi and G. Farassat, "The Prediction of Helicopter Discrete Frequency Noise," *Vertica,* vol. 7, no. 4, pp. 309-320, 1983.

[4] P. Di Francescantonio, "A New Boundary Integral Formulation for the Prediction of Sound Radiation," *Journal of Sound and Vibration,* vol. 202, no. 4, pp. 491-509, 1997.

[5] G. Rahier, "Comparison of surface and volume integral methods for transonic propeller acoustic predictions," *Computers and Fluids*, vol. 179, pp. 178-193, 2018.

[6] A. Hajczak, L. Sanders, F. Vuillot and P. Druault, "Investigation of the Ffowcs-Williams and Hawkings Analogy on an Isolated Landing Gear Wheel," in *AIAA AVIATION FORUM*, AIAA Paper 2018-3301, June 25-29, 2018.

[7] E. Manoha and B. Caruelle, "Summary of the LAGOON Solutions from the Benchmark problems for Airframe Noise Computations-III Workshop," in *21st AIAA/CEAS Aeroacoustics Conference*, AIAA Paper 2015-2846, June 22-26, 2015.

[8] M. L. Shur, P. R. Spalart and M. K. Strelets, "Noise Prediction for Increasingly Complex Jets. Part I: Methods and Tests," *International Journal of Aeroacoustics*, vol. 4, no. 3, 2005.

[9] D. Lockard and J. Casper, "Permeable Surface Corrections for Ffowcs Williams and Hawkings Integrals," in *11th AIAA/CEAS Aeroacoustics Conference*, AIAA Paper 2005-2995, 23-25 May, 2005.

[10] G. Rahier, M. Huet and J. Prieur, "Additional terms for the use of Ffowcs Williams and Hawkings surface integrals in turbulent flows," *Computers & Fluids*, vol. 120, pp. 158-172, 2015.

[11] T. Ikeda, S. Enomoto, K. Yamamoto and K. Amemiya, "Quadrupole Corrections for the Permeable-Surface Ffowcs Williams–Hawkings Equation," *AIAA Journal*, vol. 55, no. 7, pp. 2307-2320, 2017.

[12] N. Ricks, L. Siozos-Rousoulis, Z. Huang, F. Contino and G. Ghorbaniasl, "A correction technique for spurious signals from the permeable Ffowcs Williams-Hawkings equation," in *AIAA/CEAS Aeroacoustics Conference*, AIAA Paper 2018-3779, June 25-29, 2018.

[13] Y. Mao and Z. Hu, "Analysis of spurious sound due to vortical flow through permeable surfaces," *Aerospace Science and Technology*, vol. 96, p. 105544, 2020.

[14] Z. Zhou, H. Wang and S. Wang, "Simplified permeable surface correction for frequency-domain Ffowcs Williams and Hawkings integrals," *Theoretical and Applied Mechanics Letters*, vol. 11, no. 4, p. 100259, 2021.

[15] S. Mendez, M. Shoeybi, S. Lele and P. Moin, "On the Use of the Ffowcs Williams-Hawkings Equation to Predict Far-Field Jet Noise from Large-Eddy Simulations," *International Journal of Aeroacoustics*, vol. 12, no. 1-2, pp. 1-20, 2013.

[16] P. Spalart, K. Belyaev, M. Shur, M. Strelets and A. Travin, "On the differences in noise predictions based on solid and permeable surface Ffowcs Williams–Hawkings integral solutions," *International Journal of Aeroacoustics*, vol. 18, no. 6-7, pp. 621-646, 2019.

[17] B. König, E. Fares, P. Ravetta and M. R. Khorrami, "A Comparative Study of Simulated and Measured Main Landing Gear Noise for Large Civil Transports," in *AIAA AVIATION FORUM*, AIAA Paper 2017-3013, June 5-9, 2017.

[18] E. Fares, B. König and M. R. Khorrami, "Effect of Geometric Granularity on the Noise Signature of a Full-Scale Large Civil Transport Nose Landing Gear," in *AIAA AVIATION FORUM*, AIAA Paper 2021-2134, August 2-6, 2021.

[19] R. Ferris, J. Appelbaum and M. R. Khorrami, "Simulations of a Full-Scale Aircraft with Installed Airframe Noise Reduction Technologies," in *AIAA AVIATION FORUM*, AIAA Paper 2018-2974, June 25-29, 2018.

[20] M. R. Khorrami, P. Ravetta, D. Lockard, B. Duda and R. Ferris, "Comparison of Measured and Simulated Acoustic Signatures for a Full-Scale Aircraft with and without Airframe Noise Abatement," in *AIAA AVIATION FORUM*, AIAA Paper 2018-2975, June 25-29, 2018.

[21] B. Duda, R. Ferris and M. R. Khorrami, "Simulation-Based Assessment of a Full-Scale Installed Quiet Landing Gear," in *25th AIAA/CEAS Aeroacoustics Conference*, AIAA Paper 2019-2476, 20-23 May, 2019.

[22] M. R. Khorrami, P. Ravetta, D. Lockard, B. Duda and R. Ferris, "Measured and Simulated Acoustic Signature of a Full-Scale Aircraft with Airframe Noise Reduction Technology Installed," in *25th AIAA/CEAS Aeroacoustics Conference*, AIAA Paper 2019-2477, 20-23 May, 2019.

[23] M. R. Khorrami, B. König, E. Fares, A. Ribeiro, M. Czech and P. A. Ravetta, "Airframe Noise Simulations of a Full-Scale Large Civil Transport in Landing Configuration," in *AIAA AVIATION FORUM*, AIAA Paper 2021-2161, August 2-6, 2021.

[24] M. Czech, L. Brusniak, M. R. Khorrami, E. Fares and a. B. König, "Comparison of Boeing 777 Airframe Noise Flight Test Data with Numerical Simulations," in *AIAA AVIATION FORUM*, AIAA Paper 2021-2162, August 2-6, 2021.

[25] P. Ravetta, M. R. Khorrami, B. König and E. Fares, "Multiplanar Synthetic Arrays and Their Application to Full-Scale Landing Gear Noise Source Identification," in *AIAA AVIATION FORUM*, AIAA Paper 2021-2163, August 2-6, 2021.

[26] R. Ferris, M. Sacks, D. Cerizza, A. Ribeiro and M. R. Khorrami, "Aeroacoustic Computations of a Generic Low Boom Concept in Landing Configuration: Part 1 - Aerodynamic Simulations," in *AIAA AVIATION FORUM*, AIAA Paper 2021-2195, August 2-6 2021, 2021.

[27] A. Ribeiro, R. Ferris and M. R. Khorrami, "Aeroacoustic Computations of a Generic Low Boom Concept in Landing Configuration: Part 2 - Airframe Noise Simulations," in *AIAA AVIATION FORUM*, AIAA Paper 2021-2196, August 2-6, 2021.

[28] M. R. Khorrami, P. Shea, C. Winski, P. Ravetta, A. Ribeiro, R. Ferris and M. Sacks, "Aeroacoustic Computations of a Generic Low Boom Concept in Landing Configuration: Part 3 - Aerodynamic Validation and Noise Source Identification," in *AIAA AVIATION FORUM*, AIAA Paper 2021-2197, August 2-6, 2021.

[29] S. Chen and G. Doolen, "Lattice Boltzmann Method for Fluid Flows," *Annual Review of Fluid Mechanics,* vol. 30, pp. 329-364, 1998.

[30] H. Chen, S. Chen and W. H. Matthaeus, "Recovery of the Navier-Stokes equations using a lattice-gas Boltzmann method," *Physical Review A,* no. 45, pp. R5339-R5342, 1992.

[31] H. Chen, "Volumetric Formulation of the Lattice-Boltzmann Method for Fluid Dynamics: Basic Concept," *Physical Review E,* vol. 58, no. 3, pp. 3955-3963, 1998.

[32] A. Anagnost, A. Alajbegovic, H. Chen, D. Hill, C. Teixeira and K. Molvig, "Digital Physics Analysis of the Morel Body in Ground Proximity," SAE Paper 970139, 1997.

[33] H. Chen, C. Texeira and K. Molvig, "Realization of Fluid Boundary Condition via Discrete Boltzmann Dynamics," *Int. Journal of Modern Physics C,* pp. 1281-1292, 1998.

[34] H. Chen, S. Kandasamy, S. Orszag, R. Shock, S. Succi and V. Yakhot, "Extended Boltzmann Kinetic Equation for Turbulent Flows," *Science,* no. 301, pp. 633-636, 2003.

[35] V. Yakhot and S. Orszag, "Renormalization Group Analysis of Turbulence," *Journal of Scientific Computing,* vol. 1, no. 2, pp. 3-51, 1986.

[36] P. Lew, P. Gopalakrishnan, D. Casalino, R. Shock, Y. Li, R. Zhang, H. Chen, K. Habibi and L. Mongeau, "An Extended Lattice Boltzmann Methodology for High Subsonic Jet Noise Prediction," in *20th AIAA/CEAS Aeroacoustics Conference*, AIAA Paper 2014-2755, 16-20 June, 2014.

[37] G. A. Brès, F. Pérot and D. M. and Freed, "A FfowcsWilliams–Hawkings Solver for Lattice–Boltzmann Based Computational Aeroacoustics," in *16th AIAA/CEAS Aeroacoustics Conference*, AIAA Paper 2010-3711, 7-9 June, 2010.

[38] D. Casalino, "An Advanced Time Approach for Acoustic Analogy Predictions," *Journal of Sound and Vibration,* vol. 261, no. 4, pp. 583-612, 2003.

[39] A. Najafi-Yazdi, G. Brès and L. Mongeau, "An Acoustic Analogy Formulation for Moving Sources in Uniformly Moving Media," *Proceedings of The Royal Society of London A,* vol. 467, no. 2125, pp. 144-165, 2011.

[40] D. Lockard, *Private communication.*

[41] AVEC, "AVEC Phased Array Software, Version 5.10," [Online]. Available: http://www.avec-engineering.com/products.html. [Accessed October 2021].

[42] T. J. Mueller, Aeroacoustic Measurements, Springer, 2002.

[43] P. Sijtsma, "CLEAN Based on Spatial Source Coherence," *International Journal of Aeroacoustics,* vol. 6, no. 4, 2007.